The loss of Bcl-6 expressing T follicular helper cells and the absence of germinal centers in COVID-19

Naoki Kaneko[1]*, Hsiao-Hsuan Kuo[1]*, Julie Boucau[1]* , Jocelyn R. Farmer[1]*, Hugues Allard-Chamard[1,4], Vinay S. Mahajan[1,2], Alicja Piechocka-Trocha[1,6], Kristina Lefteri[1], Matt Osborn[1], Julia Bals[1], Yannic C. Bartsch[1], Nathalie Bonheur[1], Timothy M. Caradonna[1], Josh Chevalier[1], Fatema Chowdhury[1], Thomas J. Diefenbach[1], Kevin Einkauf[1], Jon Fallon[1], Jared Feldman[1], Kelsey K. Finn[1], Pilar Garcia-Broncano[1], Ciputra Adijaya Hartana[1], Blake M. Hauser[1], Chenyang Jiang[1], Paulina Kaplonek[1], Marshall Karpell[1], Eric C. Koscher[1], Xiaodong Lian[1], Hang Liu[1], Jinqing Liu[1], Ngoc L. Ly[1], Ashlin R. Michell[1], Yelizaveta Rassadkina[1], Kyra Seiger[1], Libera Sessa[1], Sally Shin[1], Nishant Singh[1], Weiwei Sun[1], Xiaoming Sun[1], Hannah J. Ticheli[1], Michael T. Waring[1,6], Alex L. Zhu[1], Jonathan Li[3], Daniel Lingwood[1], Aaron G. Schmidt[1,5], Matthias Lichterfeld[1,3], Bruce D. Walker[1,6,7], Xu Yu[1], Robert F Padera, Jr.[2#], Shiv Pillai[1#] and the Massachusetts Consortium on Pathogen Readiness Specimen Working Group[&]

[1] Ragon Institute of MGH, MIT and Harvard, Cambridge, MA 02139, USA
[2] Department of Pathology, Brigham and Women's Hospital, Boston, MA 02115
[3] Department of Medicine, Brigham and Women's Hospital, Boston, MA 02115
[4] Division of Rheumatology, Faculté de médecine et des sciences de la santé de l' Université de Sherbrooke et Centre de Recherche Clinique Étienne-Le Bel, Sherbrooke, Québec, J1K 2R1, Canada
[5] Department of Microbiology, Harvard Medical School, Boston, MA 02115
[6] Howard Hughes Medical Institute, Chevy Chase MD, 20815
[7] Department of Biology and Institute of Medical Engineering and Science, Massachusetts Institute of Technology, Cambridge, MA 02139

*Equal contributors

Correspondence to pillai@helix.mgh.harvard.edu (SP) and padera@rics.bwh.harvard.edu (RFP)
Head Lead: SP

Graphical Abstract

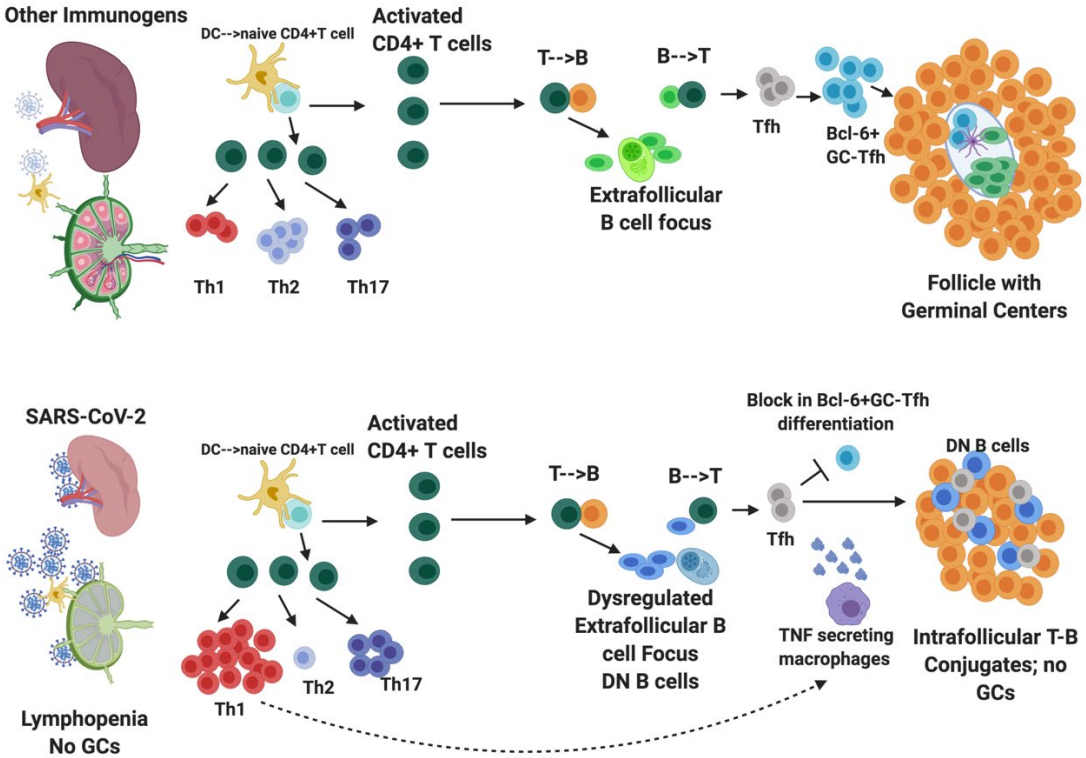

In Brief

In lymph nodes and spleens in acute COVID-19 there is a striking loss of germinal centers, depletion of Bcl-6$^+$ B cells but preservation of AID$^+$ B cells. A specific block in germinal center type Bcl-6$^+$ T follicular helper cell differentiation explains the loss of germinal centers and the accumulation of non-germinal center derived activated B cells. These data provide a mechanism for the lower quality and lack of durability of humoral immune responses observed during natural infection with SARS-CoV-2 and have significant implications for expectations of herd immunity.

Highlights

- In lymph nodes and spleens in acute COVID-19, germinal centers, the sites at which a Darwinian genetic diversification and selection process normally generates high affinity and durable antibodies, are lost
- Bcl-6$^+$ GC B cells are very sparse but AID$^+$B cells are preserved
- A specific block in Bcl-6$^+$ T follicular helper cell differentiation was observed
- T_{H1} cells were predominant and aberrant TNF-α production was seen at the site of T_{FH} cell differentiation in secondary lymphoid organs
- T-B conjugates are common and non-germinal center derived activated disease-related B cells accumulate in COVID-19 lymphoid organs
- Similar SARS-CoV-2 specific activated B cells accumulate in the blood of patients

Summary

Humoral responses in COVID-19 disease are often of limited durability, as seen with other human coronavirus epidemics. To address the underlying etiology, we examined postmortem thoracic lymph nodes and spleens in acute SARS-CoV-2 infection and observed the absence of germinal centers, a striking reduction in Bcl-6^+ germinal center B cells but preservation of AID^+ B cells. Absence of germinal centers correlated with an early specific block in Bcl-6^+T_{FH} cell differentiation together with an increase in T-bet^+T_{H1} cells and aberrant extra-follicular TNF-α accumulation. Parallel peripheral blood studies revealed loss of transitional and follicular B cells in severe disease and accumulation of SARS-CoV-2-specific "disease-related" B cell populations. These data identify defective Bcl-6^+T_{FH} cell generation and dysregulated humoral immune induction early in COVID-19 disease, providing a mechanistic explanation for the limited durability of antibody responses in coronavirus infections and suggest that achieving herd immunity through natural infection may be difficult.

Introduction

Adaptive immunity is initiated in secondary lymphoid organs and is influenced by the milieu generated by the initial activation of the innate immune system. Longitudinal studies on humoral immunity in COVID -19 as well as studies in convalescent subjects indicate that humoral immunity is often short lived and that most SARS-CoV-2 antibodies exhibit limited somatic hypermutation (Long et al., 2020, Robbiani et al., 2020). Understanding how the adaptive immune system is modulated in severe COVID-19 disease thus requires interrogation of secondary lymphoid organs in the acute phase of infection, where these responses are generated, but most studies to date have largely focused on peripheral blood samples.

SARS-CoV-2 infection results in a broad spectrum of clinical manifestations from asymptomatic to rapidly fatal, but the reasons for this heterogeneity are not known. Severely ill patients experience a life-threatening acute respiratory distress syndrome, and, even in an advanced care setting, some patients sustain severe lung damage and succumb early (Zhu et al. 2020; Zhou et al., 2020). Virus is found in the lungs and airways early in infection but not as the disease progresses (Schaefer et al., 2020). Damage-associated molecular patterns (DAMPs) released by infected pneumocytes likely combine with viral pathogen-associated molecular patterns (PAMPs) to activate innate immunity (Vardhana and Wolchok, 2020). The cytokine milieu thus generated would be predicted to influence the induction of lymphocyte activation by antigen conveyed directly in the lymph or by dendritic cells to draining lymph nodes. Viremia likely also leads to the initiation of immune responses in the spleen.

Many of the features of severe human coronavirus disease in COVID-19 and in SARS are strikingly similar. Progressive lymphopenia has been described in SARS-CoV-2 infection (Guan et al., 2020) and the degree of lymphopenia has been correlated with increases in circulating IL-6

and IL-8 (Zhang et al., 2020). Lymphopenia was also observed in SARS at the peak of active disease which was also characterized by cytokine storm and acute respiratory distress (Perlman and Dandekar, 2005). Autopsy studies in SARS showed atrophy of lymphoid organs including lymph nodes, spleen and Peyer's patches and loss of germinal centers (Gu et al., 2005). Autopsy studies in COVID-19 have also identified splenic white pulp atrophy (Xu et al. 2020, Buja et al., 2020) and lymphocyte depletion in spleen and lymph nodes (Lax et al., 2020). However, numerous viral and non-viral infections do give rise to cytokine storm, acute respiratory distress and lymphopenia (Tisoncik et al., 2012). Splenic white pulp atrophy has also been histo-pathologically demonstrated in Ebola and Marburg disease (Martines et al., 2016, Rippey et. al., 1984) and in H5N1 influenza (Gao et al. 2010, Lu et al., 2008). These data, taken together, suggest that many different viral and infectious triggers can contribute to a similar constellation of immunological phenomena that may drive pathology.

In persons with COVID-19, the magnitude and durability of antibody responses are greater in those with more severe disease (Ju et al., 2020; Amanat et al., 2020) but are often of low magnitude (Robbiani et al., 2020) and appear to lack durability (Long et al., 2020). This may be similar to SARS and MERS where humoral responses were generally not durable except in a few who survived severe infections (Long et al., 2007, Mo et al., 2006, Zumla et al., 2015). Impaired infection-induced protective immunity has also been documented by repeated infections with the human coronaviruses CoV 229E, NL63, OC43 and HKU1 in patients with less severe respiratory tract infections (Galanti et al., 2018). Reinfection could be possibly attributed to viral strain subtypes, but the reason/s for the general lack of durable humoral immune responses to coronaviruses has never been established.

A better understanding of alterations to components of the humoral immune system, especially in secondary lymphoid organs, provides an opportunity to decipher why natural infections with coronaviruses often do not provide durable immunity. A granular analysis of B and T lymphocytes in draining lymph nodes and spleens of SARS or MERS patients was never reported, leaving the underlying basis for the lymphopenia and the general lack of durability of antibody responses in those diseases unresolved. Since COVID-19 disease most significantly affects the lungs, we undertook an analysis of thoracic lymph nodes examining lymphoid architecture and lymphocyte populations using multi-color immunofluorescence, multispectral imaging and cell-cell interaction analyses from the time of disease onset in persons with diverse disease outcomes. Given the viremia has been observed in this illness (Zheng et al., 2020, Lescure et al., 2020) we also interrogated spleens both in the acute and late disease settings and complemented these studies with examination of peripheral blood samples in a separate cohort wherein convalescence could also be studied. Our results identify a striking absence of lymph node and splenic germinal centers and Bcl-6 expressing B cells, defective Bcl-6+ T follicular helper cell generation and differentiation and dysregulated SARS-CoV-2 specific humoral immunity early in COVID-19 disease, providing a mechanistic explanation for the limited durability of humoral immunity and the less robust somatic hypermutation seen in this disease following natural infection.

Results

Absence of germinal centers, loss of Bcl-6$^+$ germinal center B cells but preservation of AID$^+$ B cells in lymph nodes early in COVID-19 disease

At the Ragon Institute, a human tissue imaging platform has been validated using quantitative high-resolution automated slide-scanning microscopy, using both regular and confocal approaches and multispectral imaging for approximately 110 validated human immune markers (using over 300 different antibodies), in order to interrogate human lymphoid and non-lymphoid organs at the single cell level. These approaches crucially preserve architecture over broad swaths of tissue. Thoracic lymph nodes in severely ill COVID-19 patients who succumbed in less than eight days after admission (the group designated "Early"; less than10 days from the onset of respiratory symptoms; **Table S1**), displayed a lack of germinal centers and these were also absent in those who succumbed later (15-36 days after admission, categorized as "Late") (**Fig. 1A, B**). Quantitation revealed dramatic early loss of both B and T cells, absolute numbers declining to about a third of their non-COVID-19 controls, and this persisted in late disease (**Fig.1 D, E**), though distinct T and B cell zones could always be clearly discerned. Human control lymph nodes and spleens, even from apparently healthy accident victims, always contain germinal centers possibly because of ongoing adaptive immunity initiated by commensal antigens. The absence of germinal centers in the thoracic lymph nodes of acutely ill COVID-19 patients in whose lungs we have already described very high viral loads (Schaefer et al., 2020) was particularly surprising.

Bcl-6 expressing germinal center B cells were also markedly reduced in COVID-19 but there was a preservation of AID expressing B cells, although these were diffusely distributed compared to controls (**Fig. 1C, F, G**). Analysis of spleens in this same group of individuals also

revealed a preponderance of red pulp and paucity of white pulp (**Fig. 2A, B**), a marked reduction in B and T cell numbers (**Fig. 2B, D, E**) and the absence of germinal centers with a marked reduction in Bcl-6$^+$ B cells (**Fig. 2C, F**). There was, however, very clear and quantitative preservation of AID$^+$ B cells in both early and late splenic tissue. Importantly follicular dendritic cells (FDC) were present in both lymph nodes and spleen in these patients, indicating that the lack of these cells was not contributing to the germinal center defect (**Fig. S1**). Together these data indicate that early in severe COVID-19 disease, even within ten days of the onset of respiratory symptoms, there is severe attrition in B and T cell numbers and a striking reduction in Bcl-6$^+$ B cells and the loss of germinal centers. Interestingly AID+ B cells are preserved indicating that activated helper T cells are still likely to be in frequent contact with antigen specific B cells.

COVID-related reduction in CD4$^+$CXCR5$^+$Bcl-6$^+$ germinal center T follicular helper cells

To better understand the absence of germinal centers in COVID-19, we explored the possibility that the tissue milieu might contribute to defective T follicular helper cell differentiation. In both the lymph nodes and spleen, in early as well as late disease, CD4$^+$ CXCR5$^+$ T_{FH} cells were present but diminished in numbers (**Fig. 3A, C, E and G**) but the decrease in CD4$^+$ Bcl-6$^+$ germinal center type T_{FH} (GC-T_{FH}) cells was striking (**Fig. 3B, D, F and H).** Tissue quantitation confirmed significant differences for both early and late disease compared to controls**.** Because these changes were seen both in thoracic lymph nodes and in the spleen these data are consistent with the view that circulating factors in severely ill COVID-19 patients may impair GC-type T_{FH} cell differentiation and thus abrogate the generation of germinal centers. Although in principle phenotypically defined CD4$^+$Bcl-6$^+$ T cells could

include both T_{FH} cells and T follicular regulatory cells, we stained cells simultaneously with CD4, CXCR5, FOXP3 and Bcl-6 among other markers and used multispectral imaging to establish that while there were $FOXP3^{+}$T regs present, there was no overlap in Bcl-6 and FoxP3 expression in COVID-19 secondary lymphoid organs, indicating that there are very few if any T follicular regulatory cells in COVID-19 (**Fig. S2A**). Because germinal center loss has been described in the context of cytokine storm in mouse models and linked genetically to an abundance of TNF-α (Popescu et al., 2019), we also examined activated secondary lymphoid tissues from controls and COVID-19 lymph nodes for TNF-α expression. In this case we used tonsils from non-COVID infected patients as a control for activated lymphoid tissue. While TNF-α is expressed at low levels in the follicle in controls, in COVID-19 it is expressed very abundantly both inside and outside the follicle (**Fig. S3**). These data indicate that the differentiation of activated $CD4^{+}$ T cells into GC-type Bcl-$6^{+}T_{FH}$ cells is specifically blocked in COVID-19. Given the known information, validated by genetic deletion, that implicates excessive TNF-α production in the loss of germinal centers in infected mice, the aberrant and exuberant synthesis of TNF-α at the site of T_{FH} differentiation in COVID-19 lymph nodes may contribute to the lack of germinal centers and the impaired quality and durability of the antibody response to SARS-CoV-2 in this disease.

Increased frequency of secondary lymphoid organ T_{H1} cells in severe COVID-19

We hypothesized that the reduction in GC-T_{FH} cell numbers likely reflects a block in differentiation, and next sought to determine if this reduction was specific to this particular $CD4^{+}$ T cell subset. We quantitated $CD4^{+}$ T cell subsets in the lymph nodes and spleens using the well-established transcription factors T-bet, GATA-3, RORγt and FOXP3 as key markers. In

contrast to the reduced GC-T_{FH} cell numbers, T_{H1} cells were consistently increased early and late in both the lymph nodes and spleen, whereas an increase in T_{H17} cells was more variable (**Fig. 4, S4**). In contrast, a consistent reduction in T_{H2} cells was observed (**Fig. 4**). Late in the disease FOXP3$^+$Tregs made up a large part of the population of CD4$^+$ T cells. Overall there was an increase in secondary lymphoid organ CD4$^+$T cells relative to CD8$^+$ T cells in COVID -19 secondary lymphoid organs though this was variable (**Fig. S5**). These data indicate that the defect in GC-type T_{FH} cell differentiation is specific and suggest that this defect may indirectly be linked to the strong T_{H1} response seen in this disease.

Follicular and extra-follicular T-B conjugates and IgD$^-$CD27$^-$ activated double negative B cells in COVID19 lymph nodes and spleens

The preservation in COVID-19 of AID$^+$ B cells and the relatively large proportions of CD4$^+$ CXCR5$^+$ T_{FH} cells (that do not express Bcl-6) and T_{H1} cells, both known to express CD40L, led us to hypothesize that even though there were no germinal centers, there may be frequent T-B conjugates in COVID-19 within follicles as well as in extra-follicular locations. The absence of germinal centers (most germinal center B cells are IgD$^-$CD27$^-$Bcl-6$^+$AID$^+$CXCR5$^+$ CD19$^+$ cells) offered the opportunity to directly ask whether many of the scattered activated AID$^+$ B cells inside and outside follicles in COVID-19 secondary lymphoid organs were also IgD$^-$CD27$^-$ "double negative" B cells. These cells are often observed in chronic infectious contexts including in viral infections as well as in autoimmunity (Portugal et al., 2017; Jenks et al., 2019). They are considered to be "disease-related" cells and are generally described as "extra-follicular", implying they are not derived from the germinal center reaction. At extra-follicular and

follicular sites these double negative B cells may be less capable of inducing the differentiation of the Bcl-6^{+}GC-T_{FH} cells that are required to induce germinal centers, possibly because they lack the expression of ICOSL (HAC and SP unpublished observations).

By applying computational tools to tissue imaging, which systematically quantitate the area of cytoplasmic overlap between sets of two cells of two different cell types, and use pre-determined cut-offs to assess true cell-cell interaction, we quantified the degree and intimacy of plasma membrane contacts between cells and observed the presence of numerous T-B conjugates in COVID-19 lymph nodes and spleens (**Fig. 5A, B**). The presence of $IgD^{-}CD27^{-}$ double negative cells both within and outside follicles in COVID-19 lymph nodes and spleens was clearly evident (**Fig. 5C**). IgG expressing class- switched plasmablasts were prominent both within the follicular and extra-follicular areas (**Fig. S2B**). These data indicate that in the absence of germinal center formation in COVID-19 an "extra-follicular" type of class-switched B cell response, more typical of disease rather than of long-lasting protection, predominates in secondary lymphoid organs.

Decreases in early transitional and follicular B cells in severe COVID-19 patients correlate with systemic inflammation While the interrogation of secondary lymphoid organs from autopsies helps provide snapshots regarding the sites of the induction of the immune response, we sought to obtain information from patients at different stages of the disease, including convalescence, by the use of extended flow cytometry panels for B cells and T cell subsets and by examining peripheral blood from patients. Given the observed accumulation of activated non-germinal center derived B cells such as $IgD^{-}CD27^{-}$ double negative B cells in COVID-19

lymphoid organs, we examined whether similar activated B cell populations with binding specificity for SARS-CoV-2 could be found in the circulation in persons with disparate disease severity.

Patients were divided into gradations of severity that included asymptomatic convalescence, moderate clinical disease that did not require an intensive care unit (ICU) admission or mechanical ventilatory support, and severe clinical disease that did require an ICU admission and mechanical ventilatory support (**Table S2**). Studies on freshly isolated PBMCs revealed that total $CD19^+$ B cells and early transitional T1 and T2 ($IgD^+CD27^-CD10^+$) B cells were markedly reduced in severely ill as compared to convalescent patients (**Fig. 6A, B**). Further analysis of severe COVID-19 cases stratified based on clinical laboratory levels of inflammatory markers revealed a decreased frequency of $CXCR5^+$ follicular B cells ($IgD^+CD27^-CD10^-CD73^+$; Farmer et al., 2019) in patients with maximum CRP levels > 200 mg/L (**Fig. 6C**). The loss of $CXCR5^+$ $CD73^+$ follicular B cells correlated with symptom duration at the time of blood draw and total days of hospital admission (**Fig. 6D**). These data suggest a direct association between these B cell phenotypic changes in blood and patient clinical morbidity from COVID-19. They indicate that in the milieu of severe COVID-19, B cells either develop very inefficiently in the bone marrow or are possibly generated but acquire an activated phenotype and are lost. This results in a marked reduction in follicular B cells and likely further compounds defects in humoral immunity.

Increases in activated naïve B cells, IgD$^-$CD27$^-$CXCR5$^-$ B cells and plasmablasts in severely ill COVID-19 patients correlate with systemic inflammation and are specific for SARS-CoV-2

Within the CD27$^+$ memory B cell compartment, there was a trend towards increased total switched memory (IgD$^-$) B cells; activated (CD21^{lo}) switched memory B cells and plasmablasts were significantly increased (as a proportion of all B cells) in severely ill as compared to convalescent COVID-19 patients (**Fig. 7A, B**). Within the IgD$^+$CD27$^-$ compartment, severely ill patients with COVID-19 showed an increase in a number of disease-related presumed non-germinal center derived activated B cells as compared to convalescent patients. These include activated naïve B cells (IgD$^+$CD27$^-$CD21^{lo}Cd11c^{hi}) (Kaminski et al., 2012) as well as atypical late transitional B cells (IgD$^+$CD27$^-$CD10$^-$CD73$^-$CXCR5$^-$) (**Fig.7C**). Additionally, IgD$^-$CD27$^-$ CXCR5$^-$ B cells that include populations described by Kaminski et al. based on the expression of CXCR5 and CD11c were expanded in severe COVID-19 as compared to convalescent patients (**Fig.7D**). Paralleling the trends observed with the loss of follicular B cells, the gain in circulating plasmablasts correlated with higher CRP levels and increased patient morbidity as measured by symptom duration and length of inpatient hospitalization (**Fig. 7E, F**). Plasmablast frequency additionally correlated with the numbers of circulating T follicular helper cells (**Fig. 7G**). We tested whether the activated B cell populations were specific for the SARS-CoV-2 Spike receptor binding domain (RBD) using recombinant RBD labeled separately with APC and PE fluorophores. Cells that stained with both labeled probes were considered authentic RBD-

specific B cells. This probe contains a very small fraction of all the potential antibody epitopes in SARS-CoV-2 but is highly specific for this particular virus. All the activated and mainly disease-related populations of relevance in COVID-19 were SARS-CoV-2 specific (**Fig. 7H**), establishing that they were expanded as a result of an adaptive immune response to this virus. These data establish that the aberrant non-germinal center type activated B cells that accumulate in tissues also accumulate in the blood of severely ill and convalescent COVID-19 patients and these are virus-specific B cells. Given that they bear the hallmarks of not being from germinal centers, they are therefore unlikely to provide optimal or durable humoral immunity.

Discussion

Long-lasting B cell memory and the highest affinity pathogen-specific antibodies are derived within germinal centers in secondary lymphoid organs. Germinal centers are anatomically structured to facilitate the selection of high affinity B cell with long life spans (Victora and Nussenzweig, 2012). Longevity of such responses exceeds decades for some infectious diseases and when a substantial portion of a population is infected, can contribute to herd immunity. In contrast, antibody responses to SARS-CoV-2 appear to be similar to other human coronaviruses in being short-lived (Long et al., 2020). Understanding the reasons for this decline in responses requires architectural studies of lymphoid organs from patients coupled with cell-cell interaction analyses, as well as approaches to reliably identify, quantify and physically locate the diverse immune cell types that contribute to antibody induction. Using quantitative multicolor immunofluorescence combined with multispectral imaging and cell-cell interaction analyses of autopsy specimens as well as analyses of peripheral blood samples in parallel cohorts with acute SARS-CoV-2 infection, we show evidence for dysregulated humoral immune induction early in COVID-19 including a striking absence of germinal centers in the earliest stages of infection, defective $Bcl6^{+}T_{FH}$ cell generation and aberrant lymphoid TNF-α production.

The absence of Bcl-6^{+} T follicular helper cells (and the consequent absence of germinal centers) in COVID-19 secondary lymphoid organs provides an explanation for a phenomenon anecdotally observed in autopsies of many different severe viral infections. These findings also provide a mechanistic basis for the recent descriptions of non-durable humoral immune responses, impaired humoral immunity and the low levels of somatic hypermutation in antibodies from convalescent COVID-19 patients (Long et al., 2020, Robbiani et al., 2020). The alteration of the cytokine milieu in secondary lymphoid organs in this disease likely reflects a

continuum across the spectrum of disease. While B cell activation, class switching and some low level somatic hypermutation do occur in COVID-19, the germinal center reaction is sub-optimal or totally absent and this will likely, in due course of time, be reflected in less durable class-switched antibody responses similar to those seen in SARS and MERS. These findings have some bearing on concepts such as herd immunity and immunity passports following natural infection with SARS-CoV-2. They strongly underscore the need and relevance of vaccination approaches to the prevention of COVID-19.

Severe infections by many different human viruses result in high levels of circulating cytokines and peripheral lymphopenia, but few studies have examined secondary lymphoid organs where immune responses are generated. Autopsy studies have revealed lymphoid depletion of the spleen and lymph nodes in Ebola, Marburg, and in H5N1 (Martines et al., 2015, Rippey et al., 1984., Lu et al., 2008, Gao et al., 2010). In SARS, lymphoid depletion and loss of germinal centers was also reported (Gu et al., 2005). Autopsy studies in these severe viral infections had not systematically examined lymphoid populations in secondary lymphoid organs. More detailed mechanistic studies of tissues have been undertaken in murine model systems. In a mouse model of severe malaria, germinal center responses were defective, and this was linked to a defect in T follicular helper cell differentiation (Ryg-Cornejo et al., 2016). *Ehrlichia muris* infection in mice has also been associated with the loss of germinal centers and accumulation of TNF-α, as seen in our studies, and the genetic deletion of TNF-α sufficed to restore germinal centers (Popescu et al, 2019). A mouse immunization model that involved prior generation of specific $CD4^+$ T cell memory prior to infection with lymphocytic choriomeningitis virus generated a severe cytokine storm, splenic shrinkage, loss of germinal centers and bone marrow hypocellularity suggesting that lymphopenia and lymphoid organ abnormalities may be

attributed to immune mechanisms rather than being a direct consequence of viral cytolysis (Penaloza-Macmaster, 2015). These studies in mice, taken together, suggest that significant elevation of secreted cytokines and chemokines seen in the context of protozoan, bacterial and viral infections can cause the loss of germinal centers.

The studies of Ryg-Cornejo et al. in murine malaria and our studies in COVID-19 suggest that the observed cytokine and chemokine dysregulation may block germinal center type T follicular helper cell differentiation. The contribution of TNF-α to germinal center formation as well as to the loss of germinal centers is complex and seemingly contradictory (Popescu et al., 2019). Local cytokine concentrations at the site of T follicular helper cell differentiation likely have important consequences for the germinal center reaction. The differentiation of $CD4^+Bcl\text{-}6^-$ $CXCR5^+$ pre-germinal center T_{FH} cells into $CD4^+Bcl\text{-}6^+CXCR5^+$ GC- T_{FH} cells has never been spatially interrogated but most likely occurs extra-follicularly at the T-B interface (Crotty S, 2014; Vinuesa et al., 2016). Based on our findings, we suspect that the very high local levels of TNF-α and possibly other cytokines at this location in COVID-19 lymph nodes, possibly induced downstream of T_{H1} cell activation, block the final step in T follicular helper cell differentiation. Given that $Bcl\text{-}6^+$ B cells, $Bcl\text{-}6^+$ T_{FH} cells and $Bcl\text{-}6^+$ T follicular regulatory cells are all extremely sparse or absent in COVID-19 secondary lymphoid organs, the formal possibility that excessive TNF signaling (or excessive signaling by some combination of cytokines in the extra-follicular area) negatively impacts the expression of *BCL6* either transcriptionally or post-transcriptionally also needs to be investigated. Deeper mechanistic studies can best be pursued in murine models.

Altered extra-follicular B cell activation could potentially also contribute to a defect in T follicular helper cell differentiation observed in SARS-CoV-2 infection. After the initial

activation of naive $CD4^+$ T cells by dendritic cells presenting the relevant MHC class II molecule and peptide, along with co-stimulation, these T cells activate antigen-specific B cells that present the same MHC-peptide complex and extra-follicular B cell foci are generated. It is in this vicinity that pre-germinal center T follicular helper cells are first generated, and we have shown in humans (Maehara et al., 2018) as others have in mice (Roco et al., 2019) that most isotype switching actually occurs at this location. In COVID -19 it is likely that some antibody generation occurs extra-follicularly, though we have identified IgG expressing plasmablasts both extra-follicularly as well as in the follicles bereft of germinal centers. Activated B cells expressing ICOSL provide additional differentiation signals to activated $CD4^+$ T cells to acquire high levels of CXCR5, induce the expression of Bcl-6 and migrate into the follicles as fully differentiated germinal center type T follicular helper cells, that set up the germinal center reaction. Perhaps because cytokine alterations lead to the formation of dysfunctional B cells and plasmablasts outside the follicle, activated B cells in COVD-19 may be less capable of inducing cognate T cells to differentiate into germinal center type T follicular helper cells.

It is possible that our investigations may throw some light on the mechanisms of disease progression in severe COVID-19, although a deeper understanding will likely await the acquisition of more knowledge and the development of suitable animal models. The evasion of the anti-viral aspects of innate immunity and the overly aggressive activation of inflammation by the virus likely results in an altered milieu that contributes both to the relative attenuation of $CD8^+$ T cell immunity and prevents the generation of Bcl-6^+ T follicular helper cells. As a result of the latter, the early development of high affinity antibodies that could contribute to some attenuation of viral spread may be compromised. Whether the increased $CD4^+/CD8^+$ T cell ratio we observe in lymph nodes and spleens of COVID-19 patients reflects selective activation of

$CD4^+$T cells or a preferential depletion of $CD8^+$ T cells is unclear. Why certain individuals are more prone to initial more aggressive and destructive immune responses also remains a very difficult question to address at this time. Based on our analyses, severe disease does not appear to be due to a paucity of regulatory T cells in secondary lymphoid organs at the earlier stages of the disease, though our approaches do not interrogate Treg function. The striking relative accumulation of FoxP3+ regulatory T cells that we observe late in disease could possibly reflect a homeostatic mechanism for the resolution of infection. More likely it reflects the reduced overall numbers of recirculating T cells entering lymphoid organs and the recurring activation of naive $CD4^+$ T cells into activated subsets that egress these lymphoid organs while lymphoid organ-resident regulatory T cells perhaps do not leave these sites and therefore appear to accumulate in lymph nodes and the spleen.

In summary, even in acutely ill COVID-19 patients, at a time when they have extremely high viral loads and abundant virus has been demonstrated in their lungs, there is a striking absence of germinal centers associated with a marked reduction of germinal center B cells, but preservation of AID-expressing B cells, Thus though there is robust T cell mediated activation of B cells, germinal centers do not form. The robust activation of non-germinal center type B cell responses does not give rise to long-lived memory or high affinity B cells. The underlying basis for the loss of germinal centers is best explained by the striking failure of differentiation of Bcl-6^+ T follicular helper cells likely because of dramatic changes in the extra-follicular cytokine milieu driven by T_{H1} cells and the aberrant local production of TNF-α in lymphoid organs. We believe these findings will be relevant to a range of human viral and non-viral diseases in which there is a cytokine storm, a better understanding of which will require a granular function-focused analysis of the architecture and composition of lymph nodes and spleens. We predict

that a broadly applicable common mechanistic basis similar to what we describe here will be elucidated in future studies on MERS, H1N1, Ebola, Marburg and other viral diseases.

Acknowledgments: This work was supported by NIH U19 AI110495 to SP, NIH R01 AI146779 to AGS, NIH R01AI137057 and DP2DA042422 to DL, BMH was supported by NIGMS T32 GM007753, TMC was supported by T32 AI007245. Funding for these studies from the Massachusetts Consortium of Pathogen Readiness, the Mark and Lisa Schwartz Foundation and Enid Schwartz is also acknowledged.

Author Contributions: Conceptualization (SP, RJP, NK, JRF, HK, JBo, BDW, XY); Methodology (HA-C, JRF, TD, MW); Investigation (NK, HK, JBo, AP-T,KL,MO, JBa, YB, NB, JC, FC, KE, JFa, KKF, PG-B,CH, CJ, PK, MK, XL, HL, JL, NL, ARM, YR, KS, JS, SS, NS, WS, XS, HJT, ALZ, RFP); Resources (RFP, BDW, XY, JL, VSM, DL, AGS, BMH, JFe, TMC, JBa, ML); Original Draft (SP, NK, JRF); Review/Editing (SP, BDW, NK, JRF, HK, JB, HAC); Supervision (SP, XY)

[&]*Mass CPR Specimen Working Group*: Betelihem A. Abayneh, Patrick Allen, Galit Allter, Diane Antille, Katrina Armstrong, Alejandro Balazs, Max Barbash, Siobhan Boyce, Joan Braley, Karen Branch, Katherine Broderick, George Daley, Ashley Ellman, Liz Fedirko, Keith Flaherty, Jeanne Flannery, Pamela Forde, Elise Gettings, David Golan, Amanda Griffin, Sheila Grimmel, Kathleen Grinke, Kathryn Hall, Meg Healey, Howard Heller, Deborah Henault, Grace Holland,

Chantal Kayitesi, Evan C Lam, Vlasta LaValle, Yuting LU, Sara Luthern, Jordan Marchewska, Brittni Martino, Ilan Millstrom, Noah Miranda, Christian, Nambu, Susan Nelson, Marjorie Noone, Claire O'Callaghan, Christine Ommerborn, Lois Chris Pacheco, Nicole Phan, Falisha A Porto, Alexandra Reissis, Francis Ruzicka, Edward Ryan, Katheleen Selleck, Arlene Sharpe, Christianne Sharr, Sue Slaugenhaupt, Kimberly Smith Sheppard, Elizabeth Suschana, Vivine Wilson, Daniel Worrall

REFERENCES

Amanat, F., Stadlbauer, D., Strohmeier, S., Nguyen, T.H.O., Chromikova, V., McMahon, M., Jiang, K., Arunkumar, G.A., Jurczyszak, D., Polanco, J.*, et al.* (2020). A serological assay to detect SARS-CoV-2 seroconversion in humans. Nat Med.

Buja, L.M., Wolf, D.A., Zhao, B., Akkanti, B., McDonald, M., Lelenwa, L., Reilly, N., Ottaviani, G., Elghetany, M.T., Trujillo, D.O.*, et al.* (2020). The emerging spectrum of cardiopulmonary pathology of the coronavirus disease 2019 (COVID-19): Report of 3 autopsies from Houston, Texas, and review of autopsy findings from other United States cities. Cardiovasc Pathol *48*, 107233.

Cao, W.C., Liu, W., Zhang, P.H., Zhang, F., and Richardus, J.H. (2007). Disappearance of antibodies to SARS-associated coronavirus after recovery. N Engl J Med *357*, 1162-1163.
Crotty, S. (2014). T follicular helper cell differentiation, function, and roles in disease. Immunity *41*, 529-542.

Farmer, J.R., Allard-Chamard, H., Sun, N., Ahmad, M., Bertocchi, A., Mahajan, V.S., Aicher, T., Arnold, J., Benson, M.D., Morningstar, J.*, et al.* (2019). Induction of metabolic quiescence defines the transitional to follicular B cell switch. Sci Signal *12*.

Galanti, M., Birger, R., Ud-Dean, M., Filip, I., Morita, H., Comito, D., Anthony, S., Freyer, G.A., Ibrahim, S., Lane, B.*, et al.* (2019). Longitudinal active sampling for respiratory viral infections across age groups. Influenza Other Respir Viruses *13*, 226-232.

Gao, R., Dong, L., Dong, J., Wen, L., Zhang, Y., Yu, H., Feng, Z., Chen, M., Tan, Y., Mo, Z.*, et al.* (2010). A systematic molecular pathology study of a laboratory confirmed H5N1 human case. PLoS One *5*, e13315.

Gu, J., Gong, E., Zhang, B., Zheng, J., Gao, Z., Zhong, Y., Zou, W., Zhan, J., Wang, S., Xie, Z.*, et al.* (2005). Multiple organ infection and the pathogenesis of SARS. J Exp Med *202*, 415-424.

Guan, W.J., Ni, Z.Y., Hu, Y., Liang, W.H., Ou, C.Q., He, J.X., Liu, L., Shan, H., Lei, C.L., Hui, D.S.C.*, et al.* (2020). Clinical Characteristics of Coronavirus Disease 2019 in China. N Engl J Med *382*, 1708-1720.

Jenks, S.A., Cashman, K.S., Woodruff, M.C., Lee, F.E., and Sanz, I. (2019). Extrafollicular responses in humans and SLE. Immunol Rev *288*, 136-148.

Ju, B., Zhang, Q., Ge, J., Wang, R., Sun, J., Ge, X., Yu, J., Shan, S., Zhou, B., Song, S.*, et al.* (2020). Human neutralizing antibodies elicited by SARS-CoV-2 infection. Nature.

Kaminski, D.A., Wei, C., Rosenberg, A.F., Lee, F.E., and Sanz, I. (2012). Multiparameter flow cytometry and bioanalytics for B cell profiling in systemic lupus erythematosus. Methods Mol Biol *900*, 109-134.

Lax, S.F., Skok, K., Zechner, P., Kessler, H.H., Kaufmann, N., Koelblinger, C., Vander, K., Bargfrieder, U., and Trauner, M. (2020). Pulmonary Arterial Thrombosis in COVID-19 With Fatal Outcome: Results from a Prospective, Single-Center, Clinicopathologic Case Series. Ann Intern Med.

Lescure, F.X., Bouadma, L., Nguyen, D., Parisey, M., Wicky, P.H., Behillil, S., Gaymard, A., Bouscambert-Duchamp, M., Donati, F., Le Hingrat, Q.*, et al.* (2020). Clinical and virological data of the first cases of COVID-19 in Europe: a case series. Lancet Infect Dis *20*, 697-706.
Long, Q.X., Liu, B.Z., Deng, H.J., Wu, G.C., Deng, K., Chen, Y.K., Liao, P., Qiu, J.F., Lin, Y., Cai, X.F.*, et al.* (2020). Antibody responses to SARS-CoV-2 in patients with COVID-19. Nat Med *26*, 845-848.

Lu, M., Xie, Z.G., Gao, Z.C., Wang, C., Li, N., Li, M., Shao, H.Q., Wang, Y.P., and Gao, Z.F. (2008). [Histopathologic study of avian influenza H5N1 infection in humans]. Zhonghua Bing Li Xue Za Zhi *37*, 145-149.

Maehara, T., Mattoo, H., Mahajan, V.S., Murphy, S.J., Yuen, G.J., Ishiguro, N., Ohta, M., Moriyama, M., Saeki, T., Yamamoto, H.*, et al.* (2018). The expansion in lymphoid organs of IL-4(+) BATF(+) T follicular helper cells is linked to IgG4 class switching in vivo. Life Sci Alliance *1*.
Martines, R.B., Ng, D.L., Greer, P.W., Rollin, P.E., and Zaki, S.R. (2015). Tissue and cellular tropism, pathology and pathogenesis of Ebola and Marburg viruses. J Pathol *235*, 153-174.

Mo, H., Zeng, G., Ren, X., Li, H., Ke, C., Tan, Y., Cai, C., Lai, K., Chen, R., Chan-Yeung, M.*, et al.* (2006). Longitudinal profile of antibodies against SARS-coronavirus in SARS patients and their clinical significance. Respirology *11*, 49-53.

Penaloza-MacMaster, P., Barber, D.L., Wherry, E.J., Provine, N.M., Teigler, J.E., Parenteau, L., Blackmore, S., Borducchi, E.N., Larocca, R.A., Yates, K.B.*, et al.* (2015). Vaccine-elicited CD4 T cells induce immunopathology after chronic LCMV infection. Science *347*, 278-282.

Perlman, S., and Dandekar, A.A. (2005). Immunopathogenesis of coronavirus infections: implications for SARS. Nat Rev Immunol *5*, 917-927.

Popescu, M., Cabrera-Martinez, B., and Winslow, G.M. (2019). TNF-alpha Contributes to Lymphoid Tissue Disorganization and Germinal Center B Cell Suppression during Intracellular Bacterial Infection. J Immunol *203*, 2415-2424.

Portugal, S., Obeng-Adjei, N., Moir, S., Crompton, P.D., and Pierce, S.K. (2017). Atypical memory B cells in human chronic infectious diseases: An interim report. Cell Immunol *321*, 18-25.

Rippey, J.J., Schepers, N.J., and Gear, J.H. (1984). The pathology of Marburg virus disease. S Afr Med J *66*, 50-54.

Robbiani, D.F., Gaebler, C., Muecksch, F., Lorenzi, J.C.C., Wang, Z., Cho, A., Agudelo, M., Barnes, C.O., Gazumyan, A., Finkin, S.*, et al.* (2020). Convergent antibody responses to SARS-CoV-2 in convalescent individuals. Nature.

Roco, J.A., Mesin, L., Binder, S.C., Nefzger, C., Gonzalez-Figueroa, P., Canete, P.F., Ellyard, J., Shen, Q., Robert, P.A., Cappello, J.*, et al.* (2019). Class-Switch Recombination Occurs Infrequently in Germinal Centers. Immunity *51*, 337-350 e337.

Ryg-Cornejo, V., Ioannidis, L.J., Ly, A., Chiu, C.Y., Tellier, J., Hill, D.L., Preston, S.P., Pellegrini, M., Yu, D., Nutt, S.L.*, et al.* (2016). Severe Malaria Infections Impair Germinal Center Responses by Inhibiting T Follicular Helper Cell Differentiation. Cell Rep *14*, 68-81.

Schaefer, I.M., Padera, R.F., Solomon, I.H., Kanjilal, S., Hammer, M.M., Hornick, J.L., and Sholl, L.M. (2020). In situ detection of SARS-CoV-2 in lungs and airways of patients with COVID-19. Mod Pathol.

Teijaro, J.R., Njau, M.N., Verhoeven, D., Chandran, S., Nadler, S.G., Hasday, J., and Farber, D.L. (2009). Costimulation modulation uncouples protection from immunopathology in memory T cell responses to influenza virus. J Immunol *182*, 6834-6843.

Tisoncik, J.R., Korth, M.J., Simmons, C.P., Farrar, J., Martin, T.R., and Katze, M.G. (2012). Into the eye of the cytokine storm. Microbiol Mol Biol Rev *76*, 16-32.

Victora, G.D., and Nussenzweig, M.C. (2012). Germinal centers. Annu Rev Immunol *30*, 429-457.

Vinuesa, C.G., Linterman, M.A., Yu, D., and MacLennan, I.C. (2016). Follicular Helper T Cells. Annu Rev Immunol *34*, 335-368.

Xu, X., Chang, X.N., Pan, H.X., Su, H., Huang, B., Yang, M., Luo, D.J., Weng, M.X., Ma, L., and Nie, X. (2020). [Pathological changes of the spleen in ten patients with new coronavirus infection by minimally invasive autopsies]. Zhonghua Bing Li Xue Za Zhi *49*, E014.

Zhang, X., Tan, Y., Ling, Y., Lu, G., Liu, F., Yi, Z., Jia, X., Wu, M., Shi, B., Xu, S.*, et al.* (2020). Viral and host factors related to the clinical outcome of COVID-19. Nature.

Zheng, H.Y., Zhang, M., Yang, C.X., Zhang, N., Wang, X.C., Yang, X.P., Dong, X.Q., and Zheng, Y.T. (2020). Elevated exhaustion levels and reduced functional diversity of T cells in peripheral blood may predict severe progression in COVID-19 patients. Cell Mol Immunol *17*, 541-543.

Zheng, S., Fan, J., Yu, F., Feng, B., Lou, B., Zou, Q., Xie, G., Lin, S., Wang, R., Yang, X*., et al.* (2020). Viral load dynamics and disease severity in patients infected with SARS-CoV-2 in Zhejiang province, China, January-March 2020: retrospective cohort study. BMJ *369*, m1443.

Zhou, P., Yang, X.L., Wang, X.G., Hu, B., Zhang, L., Zhang, W., Si, H.R., Zhu, Y., Li, B., Huang, C.L*., et al.* (2020). A pneumonia outbreak associated with a new coronavirus of probable bat origin. Nature *579*, 270-273.

Zhu, N., Zhang, D., Wang, W., Li, X., Yang, B., Song, J., Zhao, X., Huang, B., Shi, W., Lu, R*., et al.* (2020). A Novel Coronavirus from Patients with Pneumonia in China, 2019. N Engl J Med *382*, 727-733.

Zumla, A., Hui, D.S., and Perlman, S. (2015). Middle East respiratory syndrome. Lancet *386*, 995-1007.

Legends to Figures

Figure 1. Early loss of germinal centers and Bcl-6 expressing B cells in COVID-19 thoracic lymph nodes

(A) Hematoxylin–eosin staining of lymph nodes from early (left) and late (right) COVID-19 patients. (B) Low-power images of CD3 (red), CD19 (green), Bcl-6 (orange) and DAPI (blue) staining in a lymph node from a late COVID-19 patient (left) and control (right). (C) Representative multi-color immunofluorescence images of CD3 (red), CD19 (green), Bcl-6 (orange) and AID (purple) staining in lymph nodes from early (left) and late (middle) COVID-19 patients and controls (right). (D and E) Absolute numbers of CD19+ B cells (D) and CD3+ T cells (E) in lymph nodes from early (purple) (n = 5) and late (blue) (n = 6) COVID-19 patients and controls (green and orange) (n = 12). Controls include lymph nodes (n = 2) and tonsils (n = 10). Orange dots mark lymph nodes and green dots mark tonsils. (F and G) Relative proportion of $Bcl6^+$ B cells (F) and AID^+ B cells (G) among $CD19^+$ B cells in lymph nodes from early (purple) (n = 5) and late (blue) (n = 6) COVID-19 patients and controls (green and orange) (n = 12). LN= Lymph node. Multiple comparisons are controlled for by Kruskal-Wallis test. Error bars represent mean ±SEM. *p < 0.05; **p < 0.01; ***p < 0.001.

Figure 2. White pulp attrition, early loss of germinal centers and Bcl-6 expressing B cells in COVID-19 spleens

(A) Cross-sectional view of whole spleen and hematoxylin–eosin staining from early (left) and late (right) COVID-19 patients. (B) Low-power images of CD3 (red), CD19 (green), Bcl-6 (orange) and DAPI (blue) staining in a spleen from late COVID-19 patient (left) and control

(right). (C) Representative multi-color immunofluorescence image of CD3 (red), CD19 (green), Bcl-6 (orange) and AID (purple) staining in spleens from early (left) and late (middle) COVID-19 patients and controls (right). (D and E) Absolute numbers of $CD19^+$ B cells (D) and CD3+ T cells (E) in spleens from early (purple) (n = 4) and late (blue) (n = 6) COVID-19 patients and controls (green) (n = 7). (F and G) Relative proportion of Bcl-6^+ B cells (F) and AID^+ B cells (G) among $CD19^+$ B cells in spleens from early (purple) (n = 4) and late (blue) (n = 6) COVID-19 patients and controls (green) (n = 7). SP=Spleen. Multiple comparisons are controlled for by Kruskal-Wallis test. Error bars represent mean ±SEM. *$p < 0.05$.

Figure 3. Loss of germinal center type Bcl-6+ T follicular helper cells in COVID-19 lymph nodes and spleens

(A) Representative multi-color immunofluorescence image of CD4 (red), CXCR5 (green) and DAPI (blue) staining in lymph nodes from early (left) and late (middle) COVID-19 patients and controls (right). Arrows indicate $CD4^+$ $CXCR5^+$ T_{FH} cells. (B) Representative multi-color immunofluorescence images of CD4 (red), Bcl-6 (white) and DAPI (blue) staining in lymph nodes from early (left) and late (middle) COVID-19 patients and controls (right). Arrows indicate $CD4^+$ Bcl-6^+ GC-type T_{FH} cells. (C) Representative multi-color immunofluorescence image of CD4 (red), CXCR5 (green) and DAPI (blue) staining in spleens from early (left) and late (middle) COVID-19 patients and controls (right). (D) Representative multi-color immunofluorescence image of CD4 (red), Bcl-6 (white) and DAPI (blue) staining in spleens from early (left) and late (middle) COVID-19 patients and controls (right). (E and F) Relative proportions of $CD4^+$ $CXCR5^+$ T_{FH} cells (E) and $CD4^+$ Bcl-6^+ GC-type T_{FH} cells among $CD4^+$ T cells (F) in lymph nodes from early (purple) (n = 5) and late (blue) (n = 6) COVID-19 patients

and controls (green) (n = 10). (G and H) Relative proportions of $CD4^+$ $CXCR5^+$ T_{FH} cells (G) and $CD4^+$ Bcl-6^+ GC-type T_{FH} (H) among $CD4^+$ T cells in spleens from early (purple) (n = 4) and late (blue) (n = 6) COVID-19 patients and controls (green) (n = 7). Multiple comparisons are controlled for by Kruskal-Wallis test. Error bars represent mean ±SEM. *p < 0.05; **p < 0.01.

Figure 4. T_{H1} cells are prominent among CD4+T cell subsets in thoracic lymph nodes and spleens

(A) Representative multi-color staining showing T_{H1}, T_H2, T_{H17} and Treg cells in lymph nodes form early (left) and late (middle) COVID-19 patients and control (right). [T_{H1}: $CD4^+$ (red) T-bet^+ (light blue)] [T_{H2}: $CD4^+$ (red) $GATA3^+$ (purple)] [T_{H17}: $CD4^+$ (red) $ROR\gamma^+$ (yellow)] [Treg: $CD4^+$ (red) $FoxP3^+$ (green)]. (B) Relative proportions of T_{H1} (upper left), T_{H2} (upper right), T_{H17} (lower left) and Treg (lower right) cells among $CD4^+$ T cells in lymph nodes and spleens from early (purple) (n = 5) and late (blue) (n = 6) COVID-19 patients and controls (green) (n = 10). Multiple comparisons are controlled for by Kruskal-Wallis test. Error bars represent mean ±SEM. *p < 0.05; **p < 0.01.

Figure 5. Follicular and extra-follicular T-B conjugates and IgD^-CD27^- B cells in COVID-19 lymph nodes

(A) Immunofluorescence staining of CD3 (red), CD19 (green) and DAPI (blue) in a lymph node (top) and a spleen (bottom) in late COVID-19 patient. Arrows and arrowheads indicate $CD3^+$ T cells and $CD19^+$ B cells respectively. T cell and B cells formed close and extensive intercellular plasma membrane contacts. (B) Immunofluorescence staining (left panels) and visualization of T-B conjugates (middle and right panels) in a lymph node from a late COVID-19 patient using

the Strata Quest cell-to-cell contact application. Masks of the nuclei based on DAPI staining establish the inner boundary of the cytoplasm and the software "looks" outwards towards the plasma membrane boundary. An overlap of at least 3 pixels of adjacent cell markers was required to establish each "contact" criterion. Details are in the Methods section. Nuclei surrounded by red and green lines respectively depict $CD3^+$ T cells and $CD19^+$ B cells in T-B conjugates. (C) Representative multi-color immunofluorescence image of CD19 (red), IgD and CD27 (both in green) and DAPI (blue) staining in a lymph node from an early COVID-19 patient. IgD-/CD27- double negative B cells (red staining with no green overlap) are abundant inside the follicle and also outside. Boxed area depicts some of these cells outside the follicle.

Fig. 6. Decreased early transitional and follicular B cells in the peripheral blood of patients with severe COVID-19. Quantitation of (**A**) total CD19+ B cells and (**B**) naïve, early transitional (T1/2), and follicular (FO) B cell subsets in the peripheral blood of patients with COVID-19 at states of convalescence (n=19), moderate disease (n=5), and severe disease (n=12) as defined by the clinical criteria listed in **Table S2** as compared to healthy controls (n=4). Quantitation shown by B cell level for each individual patient with mean, standard deviation, and significance by one-way ANOVA of log % B cell value indicated (*$P < 0.05$, ***$P < 0.001$, ****$P < 0.0001$). Representative dot plots shown (**B**) with full B cell flow cytometry gating strategy outlined in **Fig. S6**. (**C**) Quantitation of naïve and FO B cell frequencies in the peripheral blood of patients with severe COVID-19 subdivided by intermediate (int, < 200 mg/L) versus high (hi, > 200 mg/L) maximum C-reactive protein (CRP) level and shown as box and whiskers plot with significance by Student's t-test of log % B cell value indicated (*$P < 0.05$). (**D**) Association of FO B cell frequency in the peripheral blood of hospitalized COVID-19 patients (moderate and severe

disease) with maximum CRP level, symptom duration at blood draw, and total length of hospital stay by linear regression with individual patients, 95% confidence bands, R^2 and *P* values shown.

Fig. 7. Increased activated B cell subsets specific for CoV-2-RBD in the peripheral blood of patients with severe COVID-19. Quantitation of (**A**) switched memory (SM) B cells, (**B**) plasmablasts, (**C**) activated naïve and CXCR5- late transitional (T3a) B cells, (**D**) double negative (DN) B cells, and (**E**, right) total (sum) activated to follicular B cell ratios in the peripheral blood of patients with COVID-19 at states of convalescence (n=19), moderate disease (n=5), and severe disease (n=12) as defined by the clinical criteria listed in **Table S2** as compared to healthy controls (n=4). Quantitation shown by B cell level for each individual patient with mean, standard deviation, and significance by one-way ANOVA of log % B cell value indicated (**P* < 0.05, ***P* < 0.01, ****P* < 0.001, *****P* < 0.0001). Representative dot plots shown with full B cell flow cytometry gating strategy outlined in **Fig. S6**. (**E**, left) Quantitation of plasmablast frequency in the peripheral blood of patients with severe COVID-19 subdivided by intermediate (int, < 200 mg/L) versus high (hi, > 200 mg/L) maximum C-reactive protein (CRP) level and shown as box and whiskers plot with significance by Student's t-test of log % B cell value indicated (*p < 0.05). (**F**) Association of plasmablast frequency in the peripheral blood of hospitalized COVID-19 patients (moderate and severe disease) with maximum CRP level, symptom duration at blood draw, and total length of hospital stay by linear regression with individual patients, 95% confidence bands, R^2 and *P* values shown. (**G**) Association of plasmablast frequency in the peripheral blood of COVID-19 patients with T follicular helper cell frequency by linear regression with individual patients (squares indicating severe disease), 95% confidence bands, R^2 and *P* values shown. Representative dot plots shown. (**H**) Summation of all CD19+ B cells binding to

CoV-2-RBD shown for n=10 convalesced and n=4 hospitalized COVID-19 patients with % CoV-2-RBD reactivity by B cell subset indicated and representative dot plots shown. % CoV-2-RBD reactivity by B cell subset per individual patient further detailed in **Fig. S7**. DN2 and DN3 Double negative B cells are CXCR5 low, while DN1 and DN4 B cells are CXCR5hi.

Figure 1

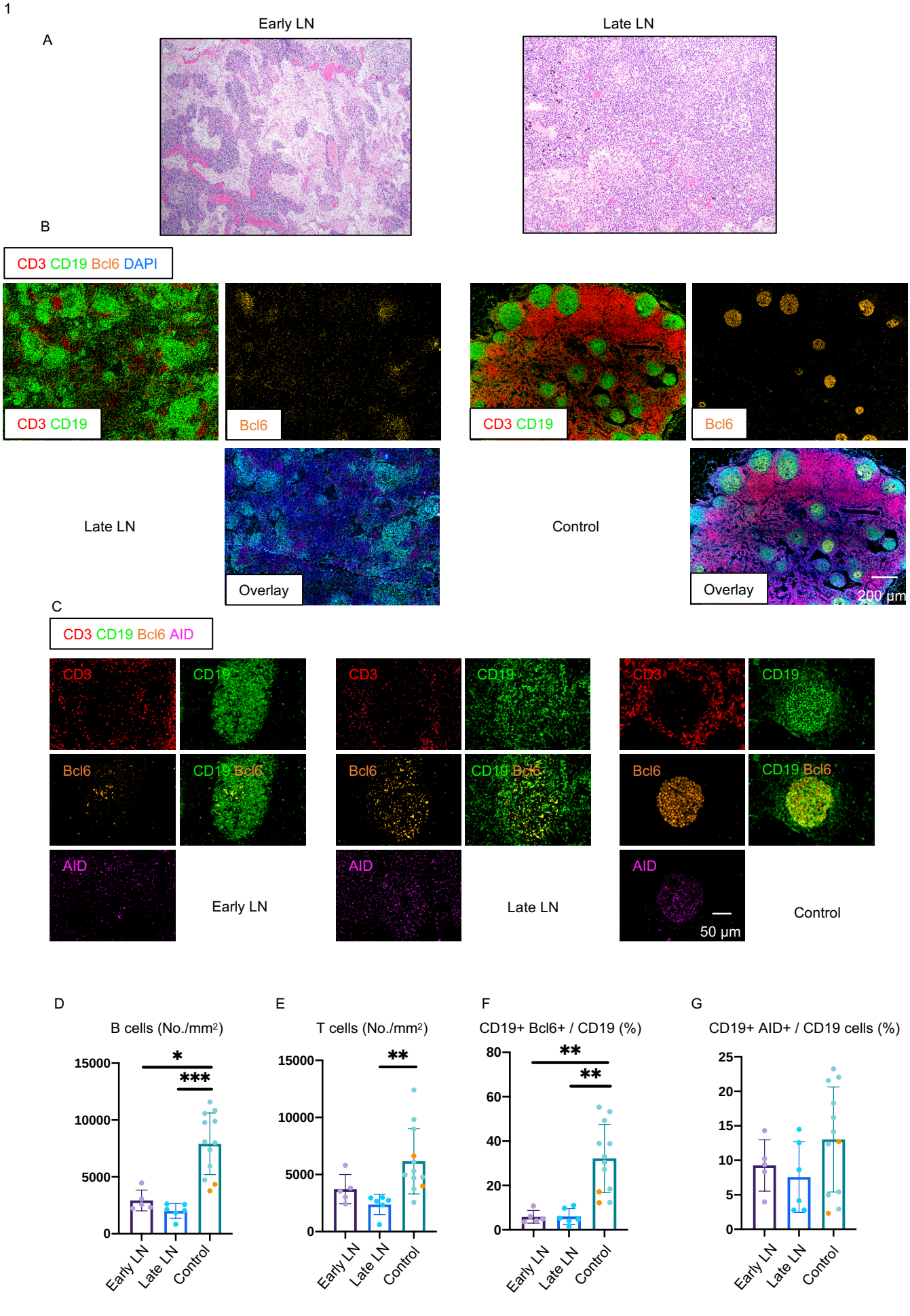
A
Early LN
Late LN
B
CD3 CD19 Bcl6 DAPI
CD3 CD19
Bcl6
Overlay
Late LN
Control
200 μm
C
CD3 CD19 Bcl6 AID
CD3
CD19
Bcl6
CD19 Bcl6
AID
Early LN
Late LN
Control
50 μm
D
B cells (No./mm²)
E
T cells (No./mm²)
F
CD19+ Bcl6+ / CD19 (%)
G
CD19+ AID+ / CD19 cells (%)
Early LN
Late LN
Control

Figure 2

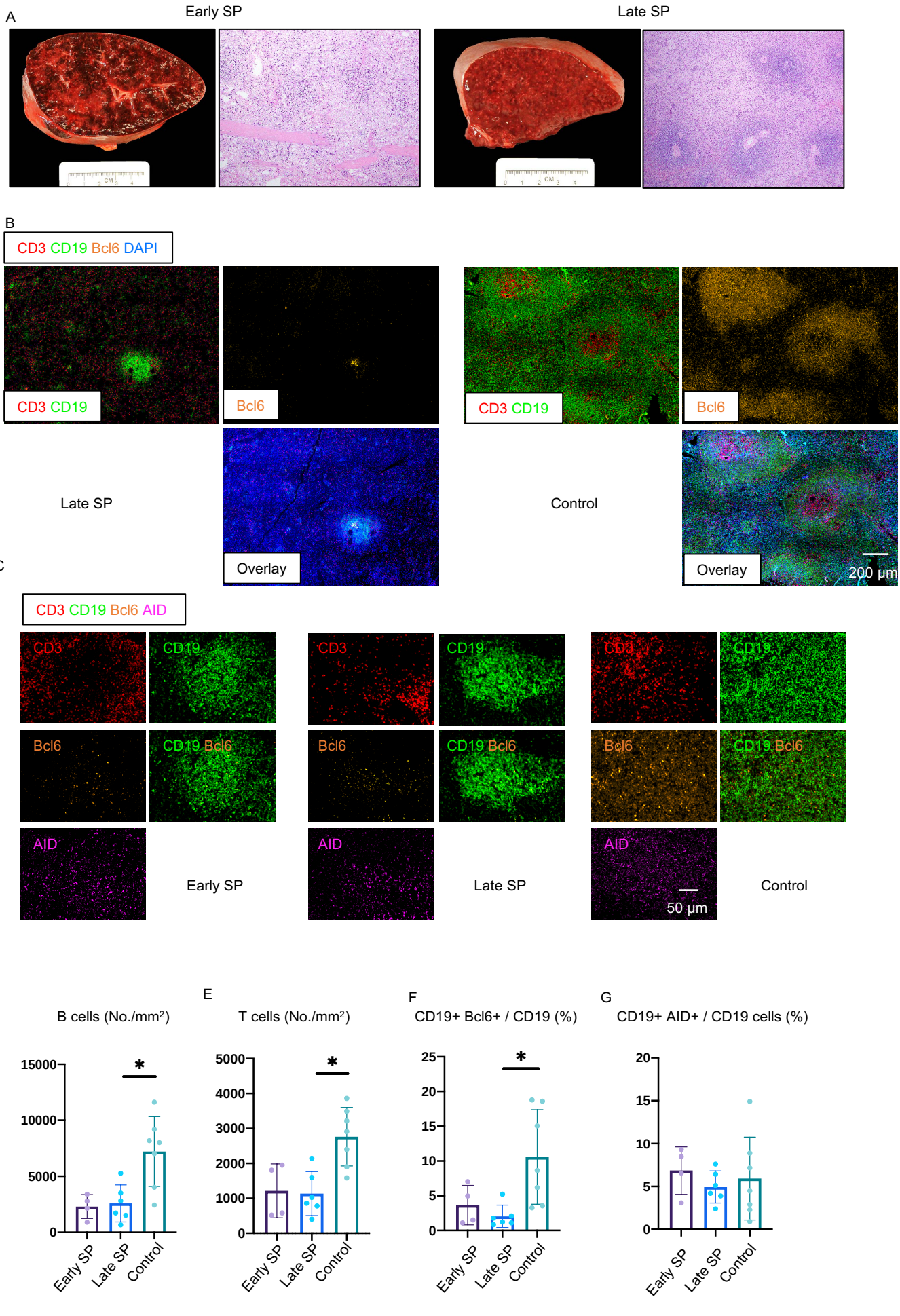
A
Early SP
Late SP
B
CD3 CD19 Bcl6 DAPI
CD3 CD19
Bcl6
Overlay
Late SP
Control
200 μm
C
CD3 CD19 Bcl6 AID
CD3
CD19
Bcl6
CD19 Bcl6
AID
Early SP
Late SP
Control
50 μm
D
B cells (No./mm²)
E
T cells (No./mm²)
F
CD19+ Bcl6+ / CD19 (%)
G
CD19+ AID+ / CD19 cells (%)
Early SP
Late SP
Control

Figure 3

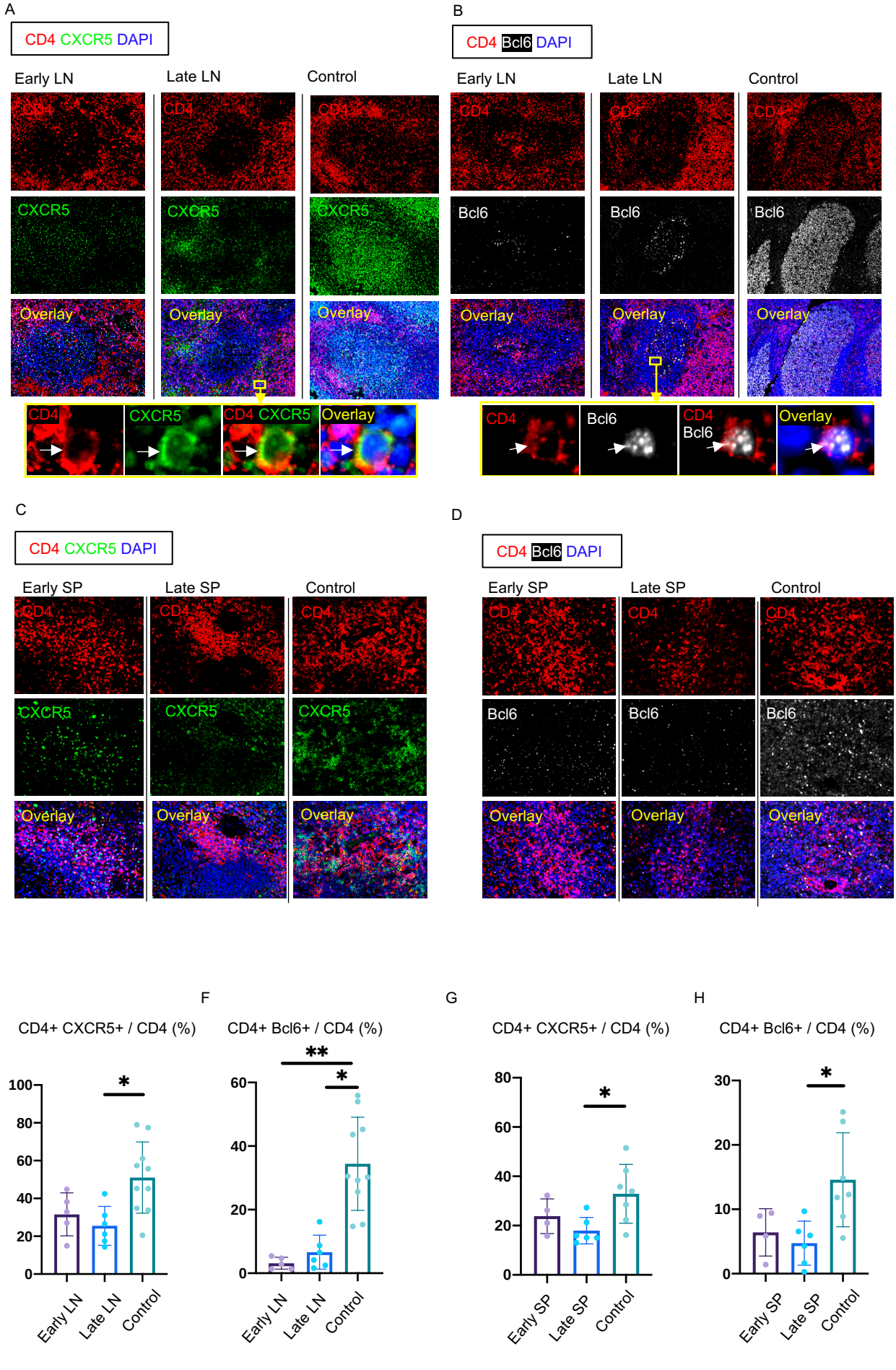
A
CD4 CXCR5 DAPI
Early LN
Late LN
Control
CD4
CXCR5
Overlay
B
CD4 Bcl6 DAPI
Early LN
Late LN
Control
CD4
Bcl6
Overlay
C
CD4 CXCR5 DAPI
Early SP
Late SP
Control
CD4
CXCR5
Overlay
D
CD4 Bcl6 DAPI
Early SP
Late SP
Control
CD4
Bcl6
Overlay
E
CD4+ CXCR5+ / CD4 (%)
100
80
60
40
20
0
*
Early LN
Late LN
Control
F
CD4+ Bcl6+ / CD4 (%)
60
40
20
0
**
*
Early LN
Late LN
Control
G
CD4+ CXCR5+ / CD4 (%)
80
60
40
20
0
*
Early SP
Late SP
Control
H
CD4+ Bcl6+ / CD4 (%)
30
20
10
0
*
Early SP
Late SP
Control

Figure 4

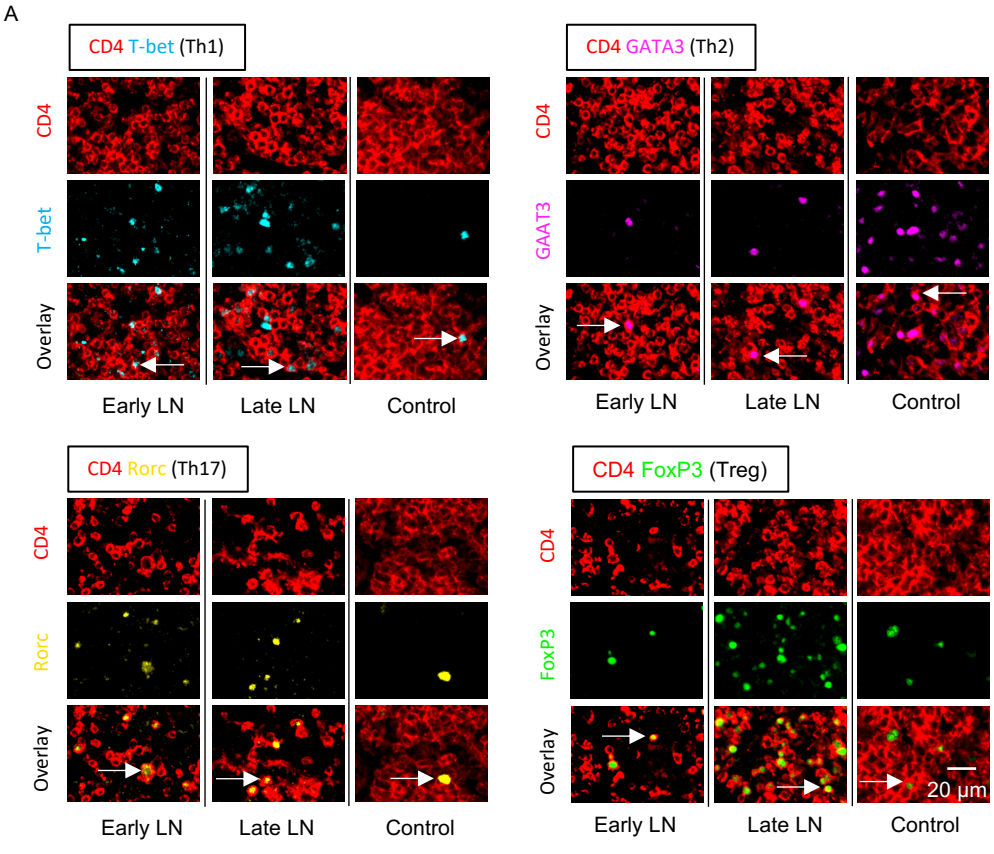
A
CD4 T-bet (Th1)
CD4
T-bet
Overlay
Early LN
Late LN
Control
CD4 GATA3 (Th2)
CD4
GAAT3
Overlay
Early LN
Late LN
Control
CD4 Rorc (Th17)
CD4
Rorc
Overlay
Early LN
Late LN
Control
CD4 FoxP3 (Treg)
CD4
FoxP3
Overlay
20 µm
Early LN
Late LN
Control

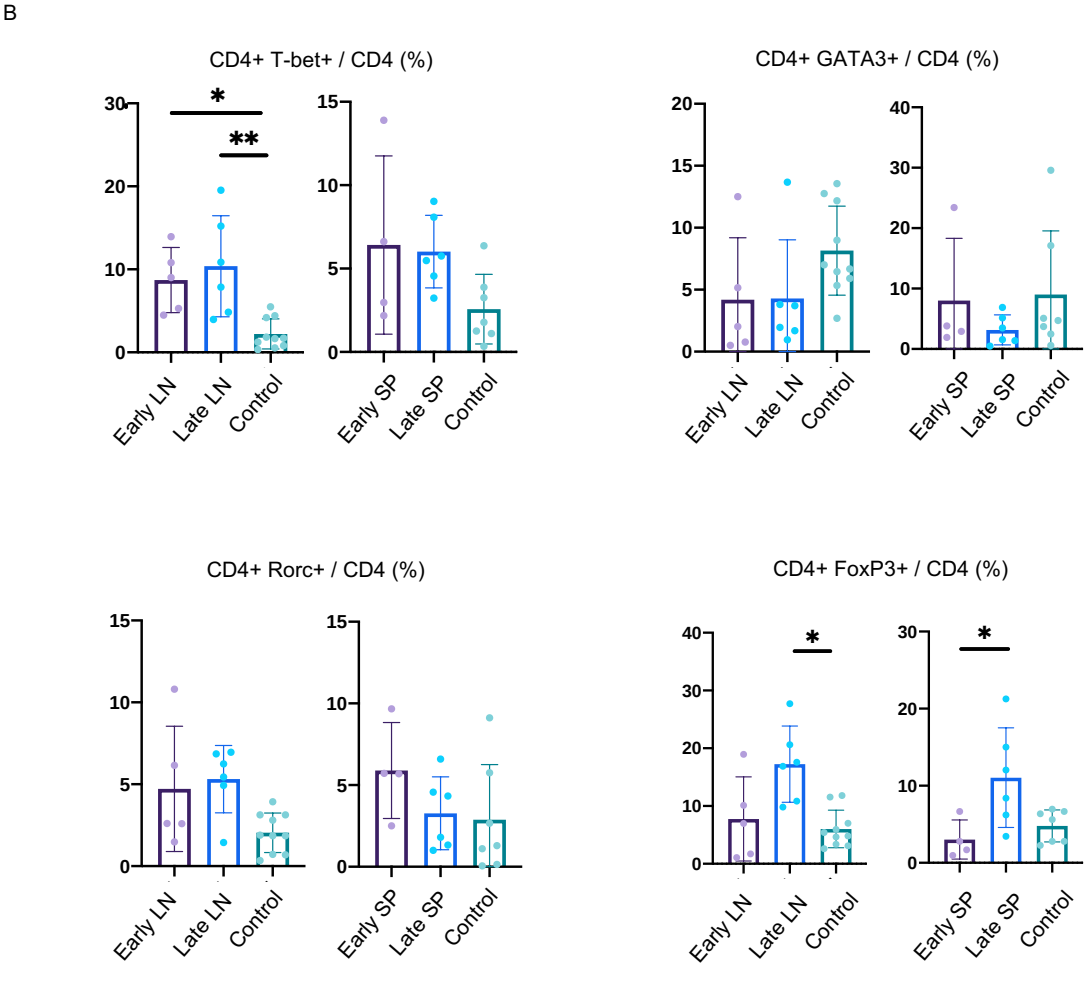
B
CD4+ T-bet+ / CD4 (%)
*
**
Early LN
Late LN
Control
Early SP
Late SP
Control
CD4+ GATA3+ / CD4 (%)
Early LN
Late LN
Control
Early SP
Late SP
Control
CD4+ Rorc+ / CD4 (%)
Early LN
Late LN
Control
Early SP
Late SP
Control
CD4+ FoxP3+ / CD4 (%)
*
*
Early LN
Late LN
Control
Early SP
Late SP
Control

Figure 5

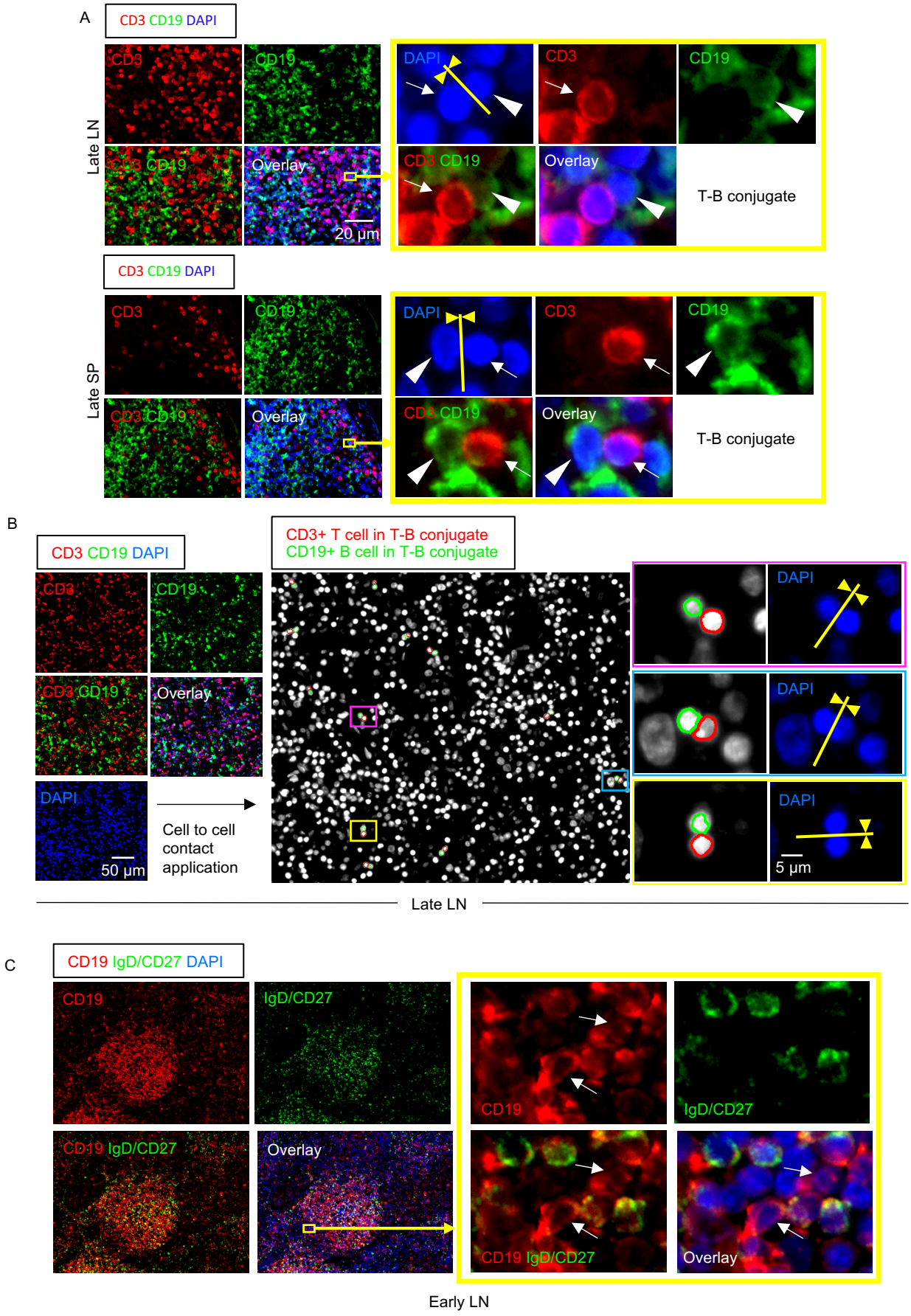
A
CD3 CD19 DAPI
Late LN
CD3
CD19
CD3 CD19
Overlay
20 μm
DAPI
T-B conjugate
Late SP
B
CD3 CD19 DAPI
CD3+ T cell in T-B conjugate
CD19+ B cell in T-B conjugate
DAPI
50 μm
Cell to cell contact application
5 μm
Late LN
C
CD19 IgD/CD27 DAPI
IgD/CD27
CD19 IgD/CD27
Overlay
Early LN

Figure 6

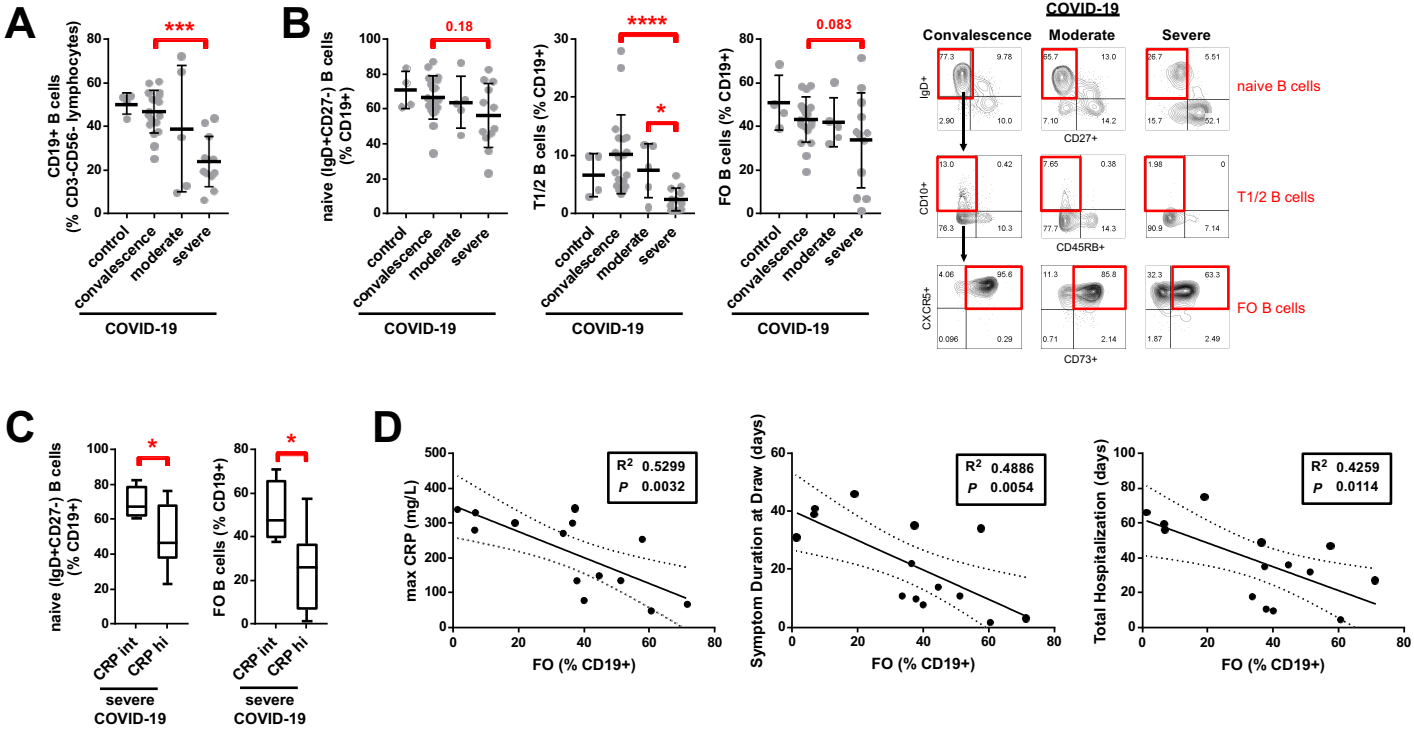
A
CD19+ B cells (% CD3-CD56- lymphocytes)
***
control
convalescence
moderate
severe
COVID-19
B
naive (IgD+CD27-) B cells (% CD19+)
0.18
T1/2 B cells (% CD19+)
****
*
FO B cells (% CD19+)
0.083
COVID-19
Convalescence
Moderate
Severe
IgD+
CD27+
CD10+
CD45RB+
CXCR5+
CD73+
naive B cells
T1/2 B cells
FO B cells
C
naive (IgD+CD27-) B cells (% CD19+)
FO B cells (% CD19+)
CRP int
CRP hi
severe COVID-19
D
max CRP (mg/L)
R2 0.5299
P 0.0032
FO (% CD19+)
Symptom Duration at Draw (days)
R2 0.4886
P 0.0054
Total Hospitalization (days)
R2 0.4259
P 0.0114

Figure 7

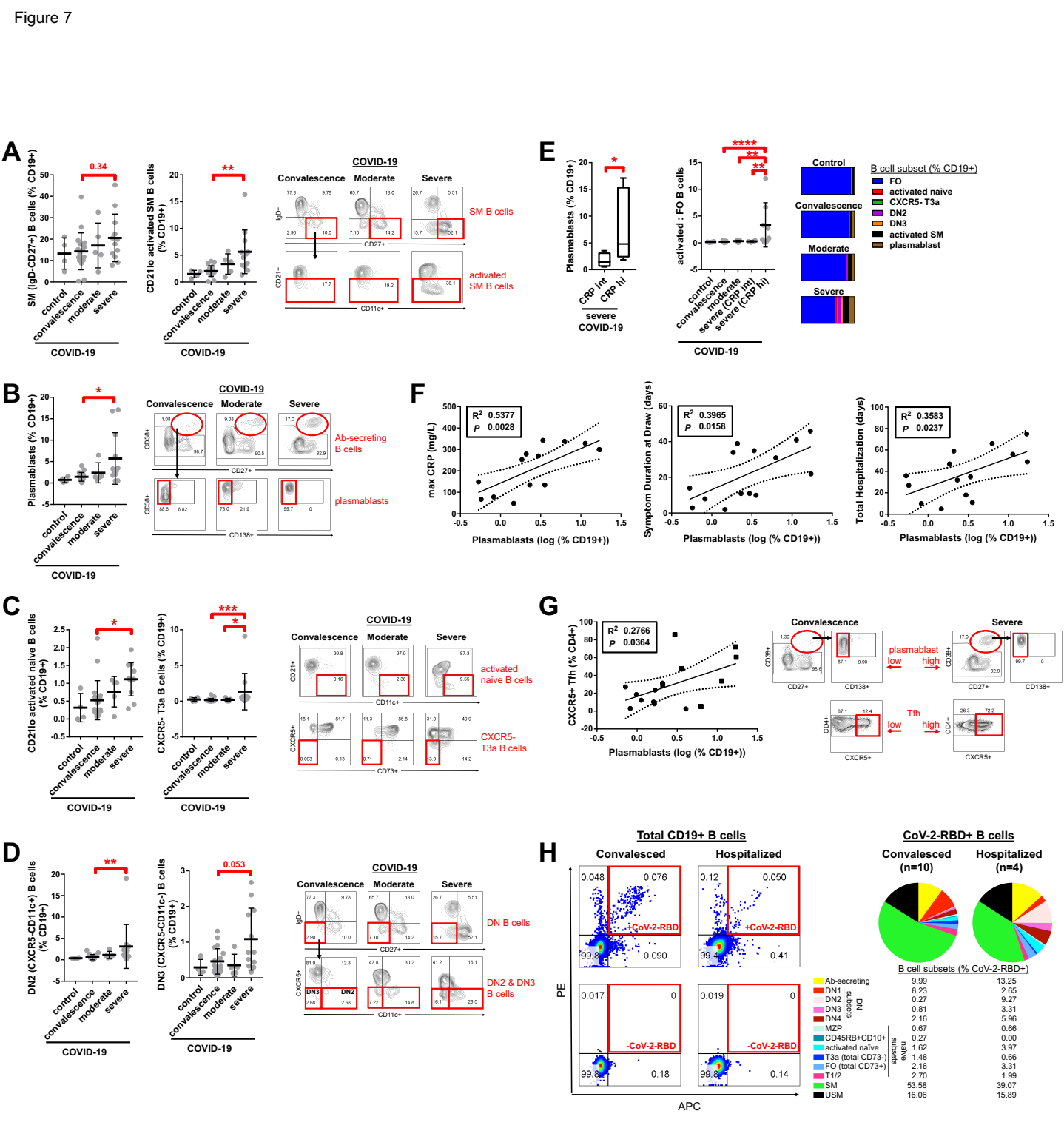
A
SM (IgD-CD27+) B cells (% CD19+)
0.34
control
convalescence
moderate
severe
COVID-19
CD21lo activated SM B cells (% CD19+)
**
COVID-19
COVID-19
Convalescence
Moderate
Severe
IgD+
CD27+
SM B cells
CD21+
CD11c+
activated SM B cells
B
Plasmablasts (% CD19+)
*
CD38+
CD27+
Ab-secreting B cells
CD138+
plasmablasts
C
CD21lo activated naive B cells (% CD19+)
*
CXCR5- T3a B cells (% CD19+)
***
*
activated naive B cells
CD73+
CXCR5- T3a B cells
D
DN2 (CXCR5-CD11c+) B cells (% CD19+)
**
DN3 (CXCR5-CD11c-) B cells (% CD19+)
0.053
DN B cells
DN2 & DN3 B cells
DN3
DN2
E
Plasmablasts (% CD19+)
*
CRP int
CRP hi
severe COVID-19
activated : FO B cells
****
**
**
severe (CRP int)
severe (CRP hi)
Control
Convalescence
Moderate
Severe
B cell subset (% CD19+)
FO
activated naive
CXCR5- T3a
DN2
DN3
activated SM
plasmablast
F
R² 0.5377
P 0.0028
max CRP (mg/L)
Plasmablasts (log (% CD19+))
R² 0.3965
P 0.0158
Symptom Duration at Draw (days)
Plasmablasts (log (% CD19+))
R² 0.3583
P 0.0237
Total Hospitalization (days)
Plasmablasts (log (% CD19+))
G
R² 0.2766
P 0.0364
CXCR5+ Tfh (% CD4+)
Plasmablasts (log (% CD19+))
Convalescence
Severe
plasmablast
low
high
CD27+
CD138+
Tfh
CD4+
CXCR5+
H
Total CD19+ B cells
Convalesced
Hospitalized
0.048
0.076
+CoV-2-RBD
99.8
0.090
0.12
0.050
+CoV-2-RBD
99.4
0.41
0.017
0
-CoV-2-RBD
99.8
0.18
0.019
0
-CoV-2-RBD
99.8
0.14
PE
APC
CoV-2-RBD+ B cells
Convalesced (n=10)
Hospitalized (n=4)
B cell subsets (% CoV-2-RBD+)
Ab-secreting 9.99 13.25
DN1 8.23 2.65
DN2 0.27 9.27
DN3 0.81 3.31
DN4 2.16 5.96
MZP 0.67 0.66
CD45RB+CD10+ 0.27 0.00
activated naive 1.62 3.97
T3a (total CD73-) 1.48 0.66
FO (total CD73+) 2.16 3.31
T1/2 2.70 1.99
SM 53.58 39.07
USM 16.06 15.89
subsets
naive

Table S1. Autopsied Patients with COVID-19 studied by immunofluorescence and multispectral imaging

Duration of hospital stay	1-8 days	16-36 days
	n=5	n=6
Clinical Course		
Hospital stay duration (days) (mean ± s.d.)	3.6 (± 3.2)	25.8 (± 7.9)
Demographics		
Age (years) (mean ± s.d.)	66.2 (± 11.2)	63.8 (± 9.3)
Gender (% male)	60%	80%
BMI (kg/m^2) (mean ± s.d.)	33.0 (± 4.1)	30.2 (± 2.0)
Maximum Laboratory Values		
CRP (mg/L) (mean ± s.d.)	199.2 (± 102.3)	74.5 (± 44.8)
LDH (U/L) (mean ± s.d.)	590.0 (± 149.9)	423.0 (± 128.2)
Ferritin (ug/L) (mean ± s.d.)	703 (± 618.0)	410.8 (± 166.1)
D-dimer (ng/mL) (range)	1374 to >4000	725 to >4000

Body mass index (BMI), C-reactive protein (CRP), lactate dehydrogenase (LDH), standard deviation (s.d.)

Table S2. Summary of information on COVID-19 patients in whom circulating B cells were analyzed by flow cytometry.

	Convalescence	**Moderate**	**Severe (CRP int)** CRP < 200 mg/L	**Severe (CRP hi)** CRP > 200 mg/L
	mean (± SD)	mean (± SD)	mean (± SD)	mean (± SD)
	n=19	n=5	n=4	n=8
Demographics				
Age (years)	44.6 (± 17.1)	46.6 (± 16.3)	59.3 (± 10.8)	59.0 (± 15.3)
Deceased (%)	0	0	0	0
Gender (% male)	42.1	40.0	100.0*	62.5
BMI (kg/m^2)	26.2 (± 4.3)	29.8 (± 9.1)	36.3 (± 7.8)**	35.3 (± 10.5)*
Clinical Course				
Hospitalized due to COVID-19 (%)	0	40	100	100
Admitted to ICU due to COVID-19 (%)	0	0	100	100
Mechanically ventilated due to COVID-19 (%)	0	0	100	100
Total Hospitalization (days)	0	3.0 (± 4.5)	26.5 (± 11.0)	50.6 (± 17.9)$^+$
Total Mechanical Ventilation (days)	0	0	20.5 (± 14.5)	36.3 (± 21.5)
Symptom Duration at Draw (days)	0	13.8 (± 10.8)	9.5 (± 4.7)	32.4 (± 11.2)$^{++}$
Convalescence Period at Draw (days)	32.3 (± 13.9)	0	0	0
Pre-Draw Immunosuppression				
Steroids (≥ prednisone 20 mg daily) (%)	na	20.0	25.0	12.5
Hydroxychloroquine (3-5 day total course) (%)	na	0	25.0	75.0
Tocilizumab (single dose or enrolled in trial) (%)	na	20.0	25.0	12.5
Maximum Laboratory Values				
CRP (mg/L)	na	64.3 (± 20.9)	122.2 (± 36.5)	301.5 (± 33.0)$^{+++}$
ESR (mm/h)	na	77.5 (± 54.4)	46.3 (± 14.9)	116.7 (± 34.3)$^{++}$
LDH (U/L)	na	323.5 (± 19.1)	670.8 (± 240.8)	762.3 (± 491.0)
Ferritin (ug/L)	na	750.0 (± 5.7)	6045.5 (± 8471.8)	2919.1 (± 3452.6)
D-dimer (ng/mL)	na	1306.0 (± 849.0)	5963.8 (± 3242.7)	8333.1 (± 2285.7)

Convalescence was defined as a clinically asymptomatic state on the date of blood draw, either from a baseline asymptomatic state or recuperated from moderate disease. Moderate disease was defined as active clinical symptoms resulting from COVID-19 infection on the date of blood draw that did not require intensive care unit (ICU) admission or mechanical ventilation for supportive care. Severe disease was defined as active clinical symptoms resulting from COVID-19 infection on the date of blood draw that did require ICU admission and mechanical ventilation for supportive care. Severe disease was further subdivided by maximum CRP level during inpatient admission as CRP < 200 mg/L 'CRP intermediate (int)' and CRP > 200 mg/L 'CRP high (hi).' Body mass index (BMI), C-reactive protein (CRP), erythrocyte sedimentation rate (ESR), lactate dehydrogenase (LDH), not available (na), standard deviation (SD), *significance by Student's t-test to 'convalescence' group, $^+$significance by Student's t-test to 'severe (CRP int)' group.

Supplementary File

Supplementary Methods
Supplementary Figures 1-7

Supplementary Methods

Patient Cohorts

Tissue analysis Cohort:

Thoracic lymph nodes and spleens samples from COVID-19 patients were obtained through the Brigham and Women's hospital Department of Pathology. All cases were retrieved from the Anatomic Pathology files of Brigham and Women's Hospital and included 11 patients with laboratory confirmed COVID-19 who underwent autopsy in 2020. All patients had tested positive for SARS-CoV-2 by RT-PCR of nasopharyngeal swabs in a laboratory during hospital admission. All cases were divided to two groups; Early (less than ten days from respiratory symptoms onsets to death, hospitalization of up to 8 days), Late (Hospitalized for 15-36 days prior to death). In addition, 2 mesenteric lymph nodes, ten healthy human tonsils and seven spleens were obtained from the Ragon Institute Tissue Core, which were histologically normal.

Peripheral Blood Cohort:

Peripheral blood samples were drawn from both Outpatients and Inpatients with COVID-19 at Massachusetts General Hospital and fresh blood was analyzed for flow cytometry using two 25 color panels from 180 patients. Data is presented on B cell populations from 36 patients, including moderately ill, severely ill and convalescent patients.

Multi-color immunofluorescence staining

Tissue samples were fixed in formalin, embedded in paraffin, and sectioned. These specimens were incubated with the following antibodies: anti-CD3 (clone: A045229-2; DAKO), anti-CD4 (clone: CM153A; Biocare Medical), anti-CD19 (clone: SKU310; Biocare Medical), anti-Bcl6

(clone: LN22; Biocare Medical), anti-AID (clone: ZA001; Invitrogen), anti-T-bet (clone: ab150440; Abcam), GATA3 (clone: CM405A; Biocare), Rorc (clone: ab212496; Abcam), CXCR5 (clone: MAB190; R&D Systems), Foxp3 (clone: 98377; Cell Signaling Technology), anti-CD8 (clone: ab85792; Abcam), anti-IgD (clone: AA093; DAKO), anti-CD27 (clone: ab131254; Abcam), anti-IgG (clone: ab109489; Abcam), anti-TNF-α (clone: ab6671; Abcam), and anti-CD35 (clone: ab25; Abcam) followed by incubation with a secondary antibody using an Opal™ Multiplex Kit (Perkin Elmer). The samples were mounted with ProLong™ Diamond Antifade mountant containing DAPI (Invitrogen).

Microscopy and Quantitative Image Analysis

Images of the tissue specimens were acquired using the TissueFAXS platform (TissueGnostics). For quantitative analysis, the entire area of the tissue was acquired as a digital grayscale image in five channels with filter settings for FITC, Cy3, Cy5 and AF75 in addition to DAPI. Cells of a given phenotype were identified and quantitated using the TissueQuest software (TissueGnostics), with cut-off values determined relative to the positive controls. This microscopy-based multicolor tissue cytometry software permits multicolor analysis of single cells within tissue sections similar to flow cytometry. In addition, multispectral images (seven-colors staining) were unmixed using spectral libraries built from images of single stained tissues for each reagent using the StrataQuest (TissueGnostics) software. StrataQuest software was also used to quantify cell-to-cell contact. In the Strata Quest cell-to-cell contact application, masks of the nuclei based on DAPI staining establish the inner boundary of the cytoplasm and the software “looks” outwards towards the plasma membrane boundary. Overlap of at least 3 pixels of adjacent cell markers is required to establish a “contact” criterion. Although the software has been developed and validated more recently, the principle of the method and the algorithms used have been described in detail elsewhere (reference Ecker RC, Steiner GE. Microscopy-based multicolor tissue

cytometry at the single-cell level. *Cytometry Part A : the journal of the International Society for Analytical Cytology*. Jun 2004;59(2):182-90. doi:10.1002/cyto.a.20052).

Flow cytometry

Fresh PBMCs were stained. Prior to antibody staining, Fc receptors were blocked using Human TruStain FcX (BioLegend, 422302) at a concentration of 1:20 on ice for 15 minutes. Cells were surface stained on ice, protected from light, using optimized concentrations of fluorochrome-conjugated primary antibodies for 30 minutes using the following antibody panel (manufacturer, clone, concentration used): CD3 (HIT3a, BioLegend), CD19 (SJ25C1, BioLegend), CD27 (M-T271, BD Biosciences), IgD (IA6-2, BioLegend), CD38 (HIT2, BD Biosciences), CD24 (ML5, BioLegend), CD10 (HI10a, BioLegend), CD45RB (MEM-55, Thermo Fisher), CD21 (B-ly4, BD Biosciences). CD73 (AD2, BioLegend),

Flow cytometry was performed on a BD Symphony (BD Biosciences, San Jose, CA) and rainbow tracking beads were used to ensure consistent signals between flow cytometry batches. FCS files were analyzed, and B cell subsets were quantified using FlowJo software (version 10). Assembly of quantified CD19+ B cell subsets and statistical analysis was performed in GraphPad Prism (version 7.01).

Statistics

Flow cytometry, clinical correlations and tissue studies. GraphPad Prism version 8 was

used for statistical analysis, curve fitting and linear regression. A two-tailed Mann-Whitney U

test was used to calculate p-values for continuous, non-parametric variables. For comparing more than one population, Kruskal-Wallis testing was used with Dunn's multiple comparison testing.

A p-value of < 0.05 was considered significant.

Study Approval

This study was performed with the approval of the Institutional Review Boards at the Massachusetts General Hospital and the Brigham and Women's Hospital.

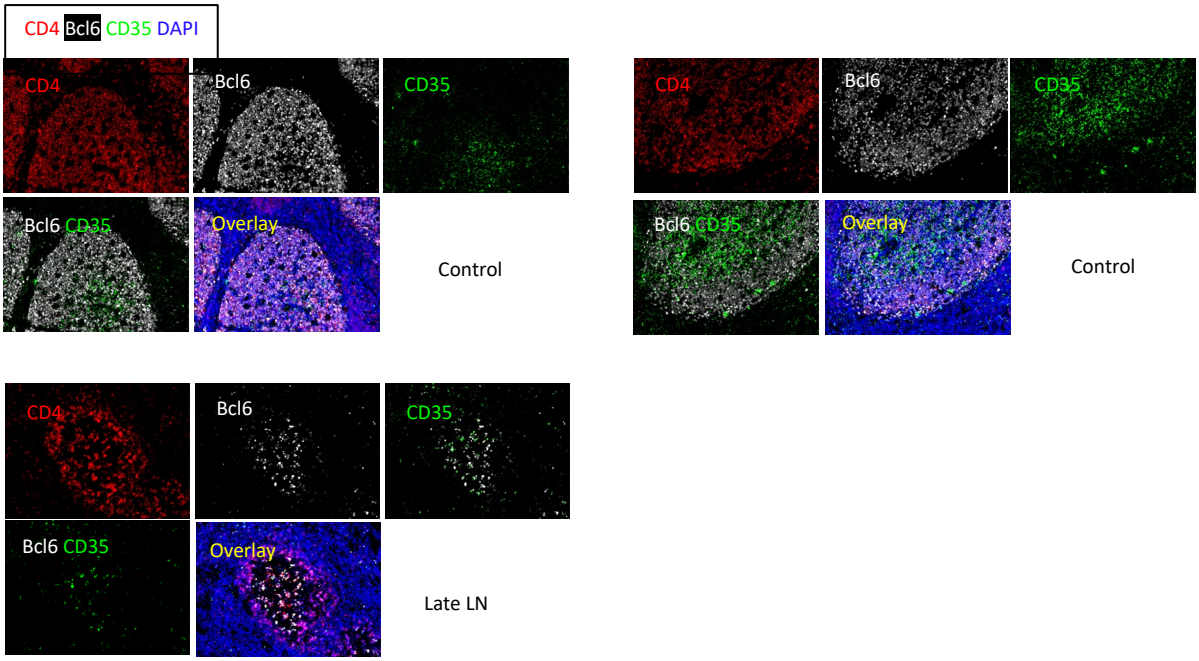

Fig. S1. No loss of FDCs in COVID-19
Representative multi-color immunofluorescence images of CD4 (red), Bcl6 (white), CD35 (green) and DAPI (blue) staining in a lymph node from late COVID-19 patients and controls.

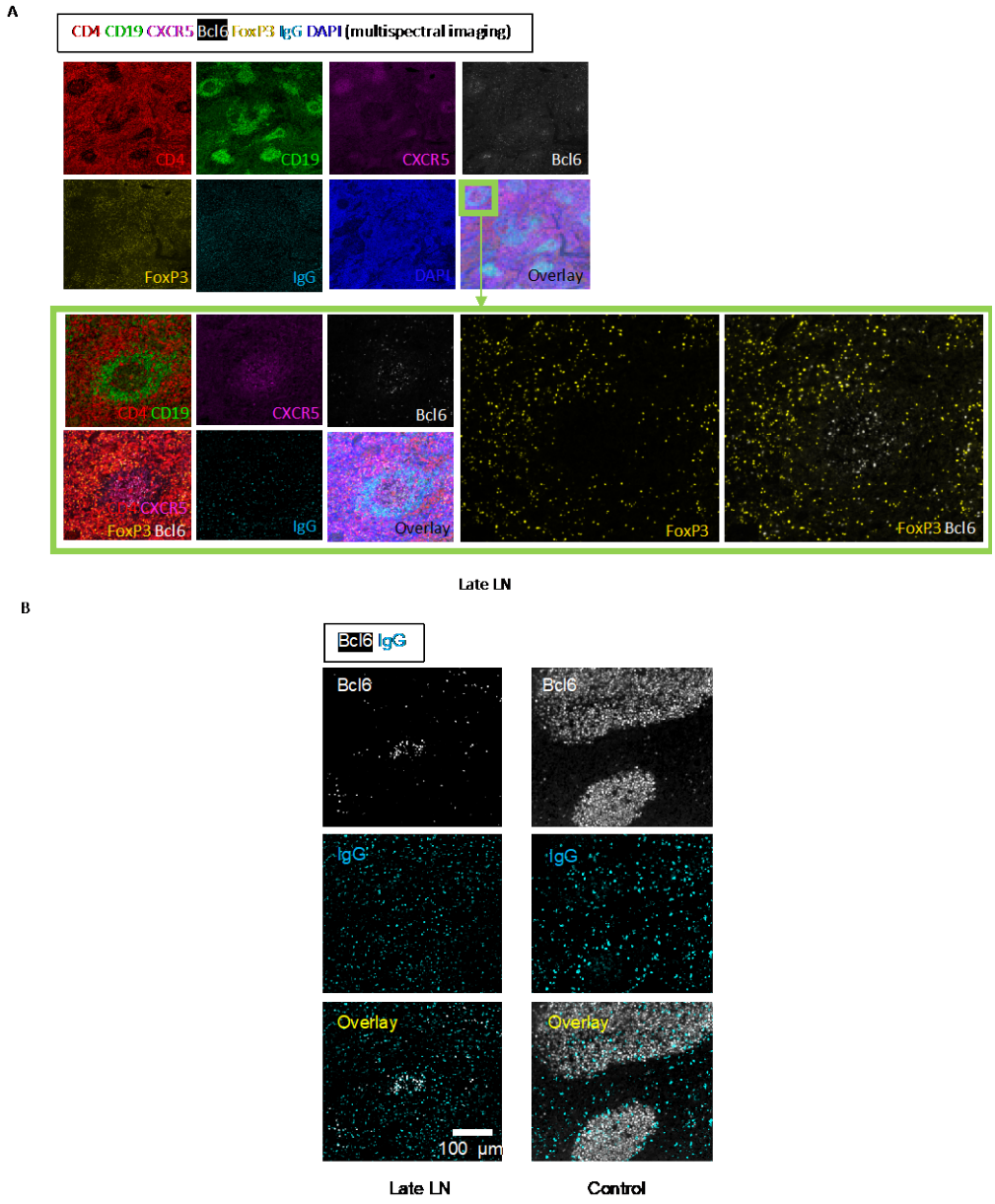

Fig. S2. A. Increased T regs but no differentiation into TFR cells late in COVID-19. Representative multi-spectral 7 colors immunofluorescence images showing CD4 (red), CD19 (green), CXCR5 (purple), Bcl6 (white) FoxP3 (yellow), IgG (light blue) and DAPI (blue) staining in lymph nodes from late COVID-19 patients. Images circled green rectangular showing high-power images of a follicle. No FoxP3+/Bcl6+ cells are seen (red staining with no green overlap) in a follicle.

B. IgG+ plasmablasts are found in follicular and extrafollicular areas in COVID-19 lymph nodes. IgG+ cells were abundant in follicular and extrafollicular areas in both COVID-19 lymph nodes and controls.

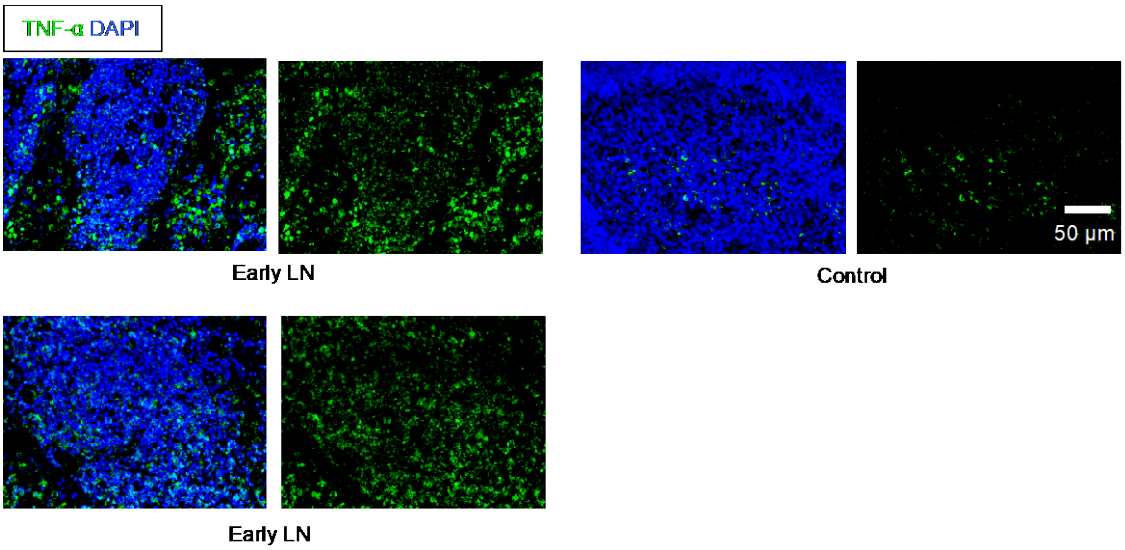

Fig. S3. Large increase in TNF-α production at both follicular and extra-follicular sites in COVID-19 lymph nodes. Controls have low levels but only in follicle
Representative multi-color immunofluorescence images of TNF-α(green) and DAPI (blue) staining in lymph nodes from early COVID-19 patients and controls.

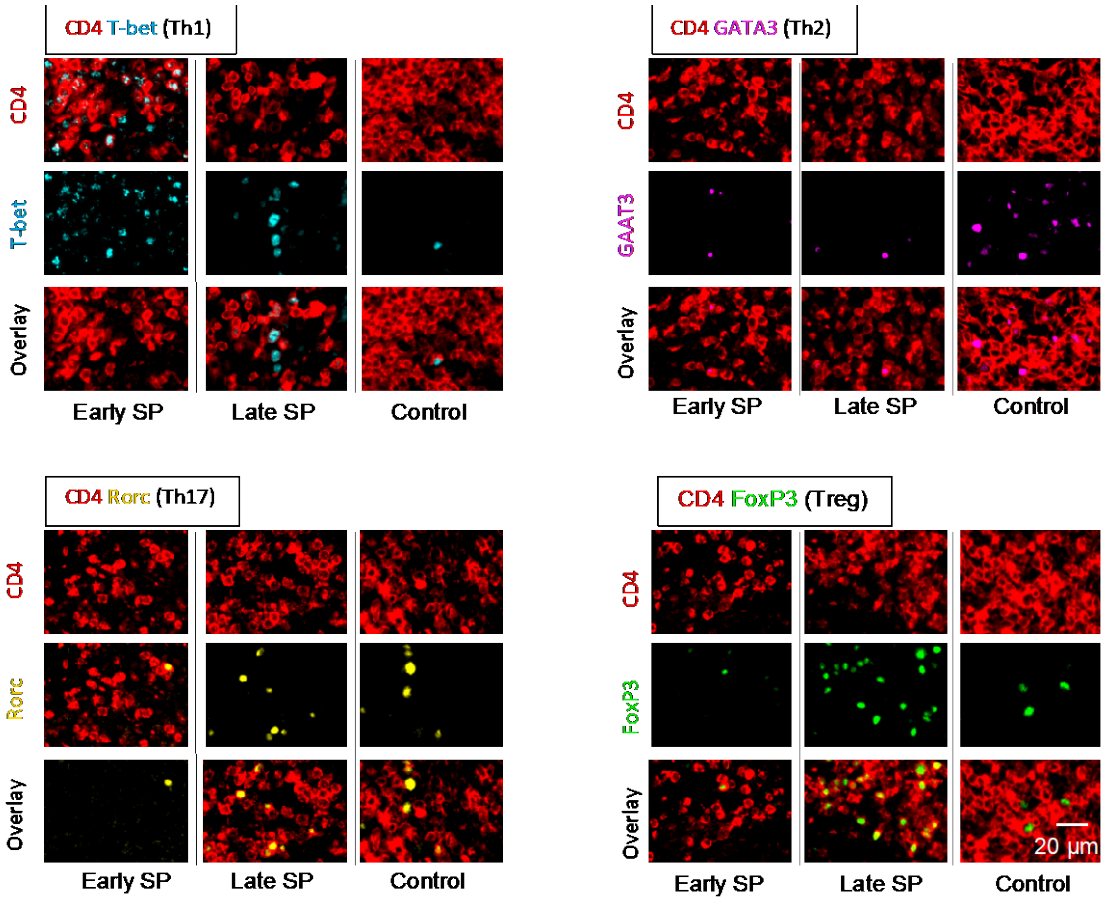

Fig. S4. Increased Th1 cells in Spleen in COVID-19
Representative multi-color staining showing T_{H1}, T_H2, T_{H17} and Treg cells in spleens from early and late COVID-19 patients and control.

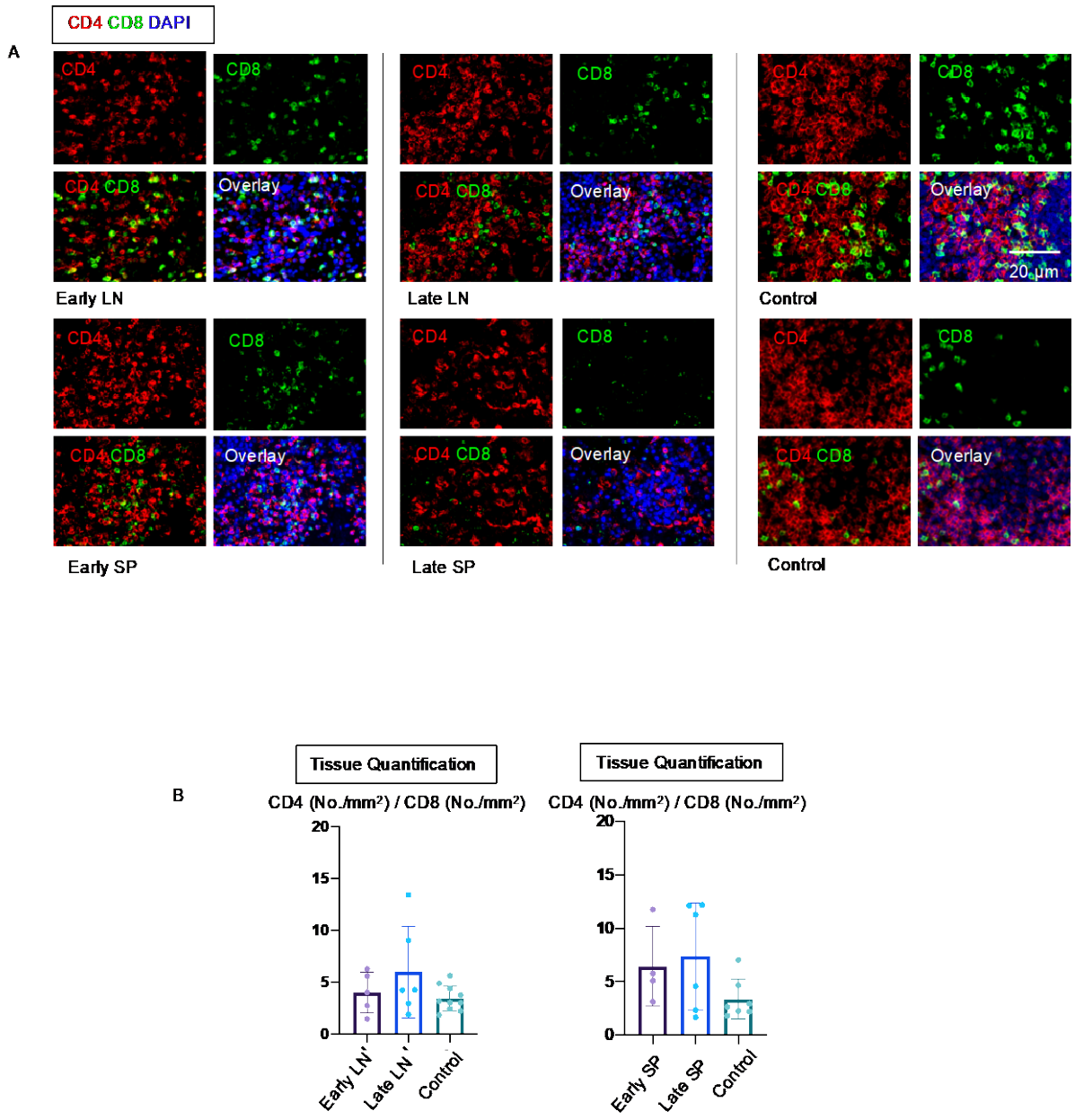

Fig. S5. Increase in CD4+/CD8+ T cell ratio in lymph nodes and spleens in COVID-19
(A) Representative multi-color immunofluorescence images of CD4 (red), CD8 (green) and DAPI (blue) staining in lymph nodes and spleens from early (left) and late (middle) COVID-19 patients and controls (right). (B) Relative ratios of CD4 and CD8 T cells (No./mm^2) in lymph nodes and spleens from early and late COVID-19 patients and controls.

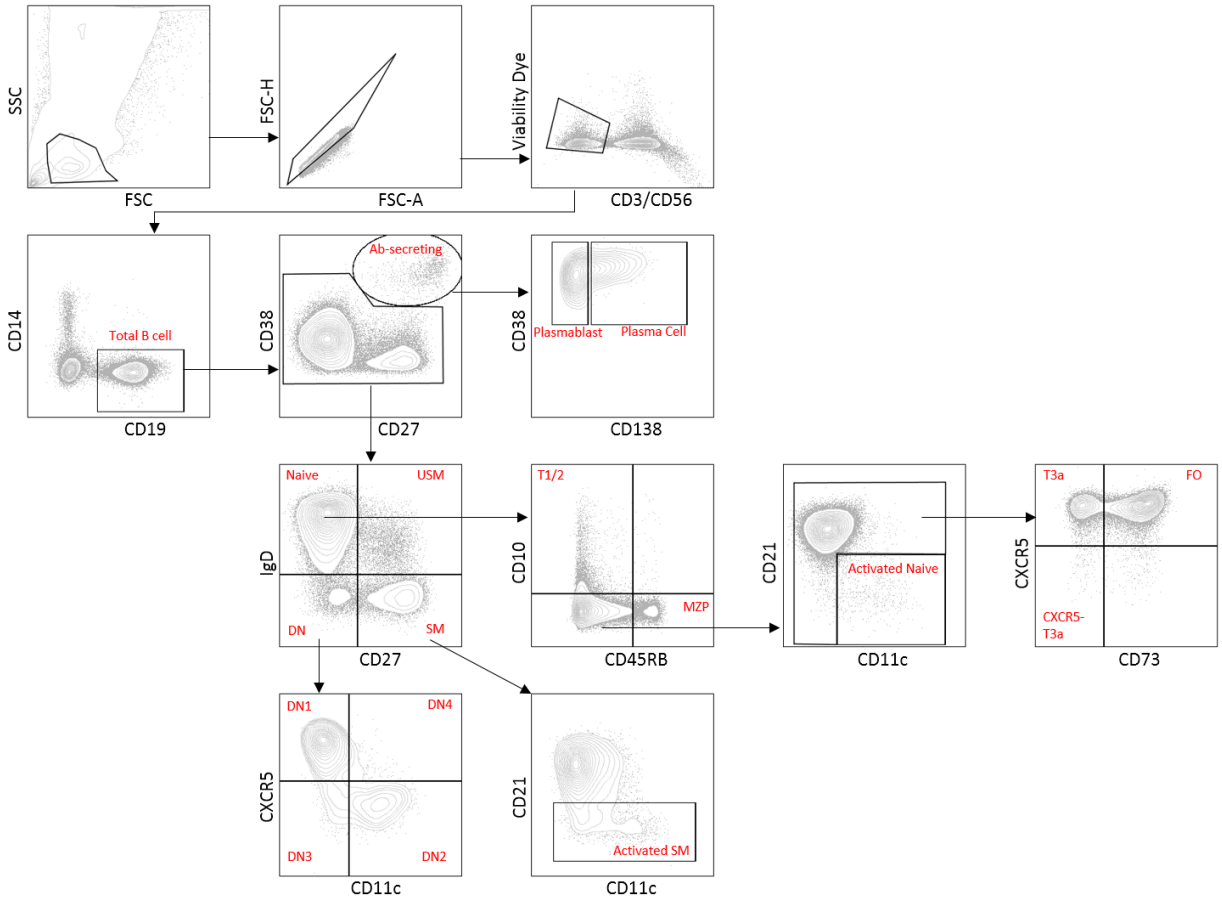

Fig. S6. B cell gating strategy for COVID-19 PBMCs. Antibody-secreting (Ab-secreting), double negative (DN), follicular (FO), marginal zone precursor (MZP), switched memory (SM), transitional (T), unswitched memory (USM).

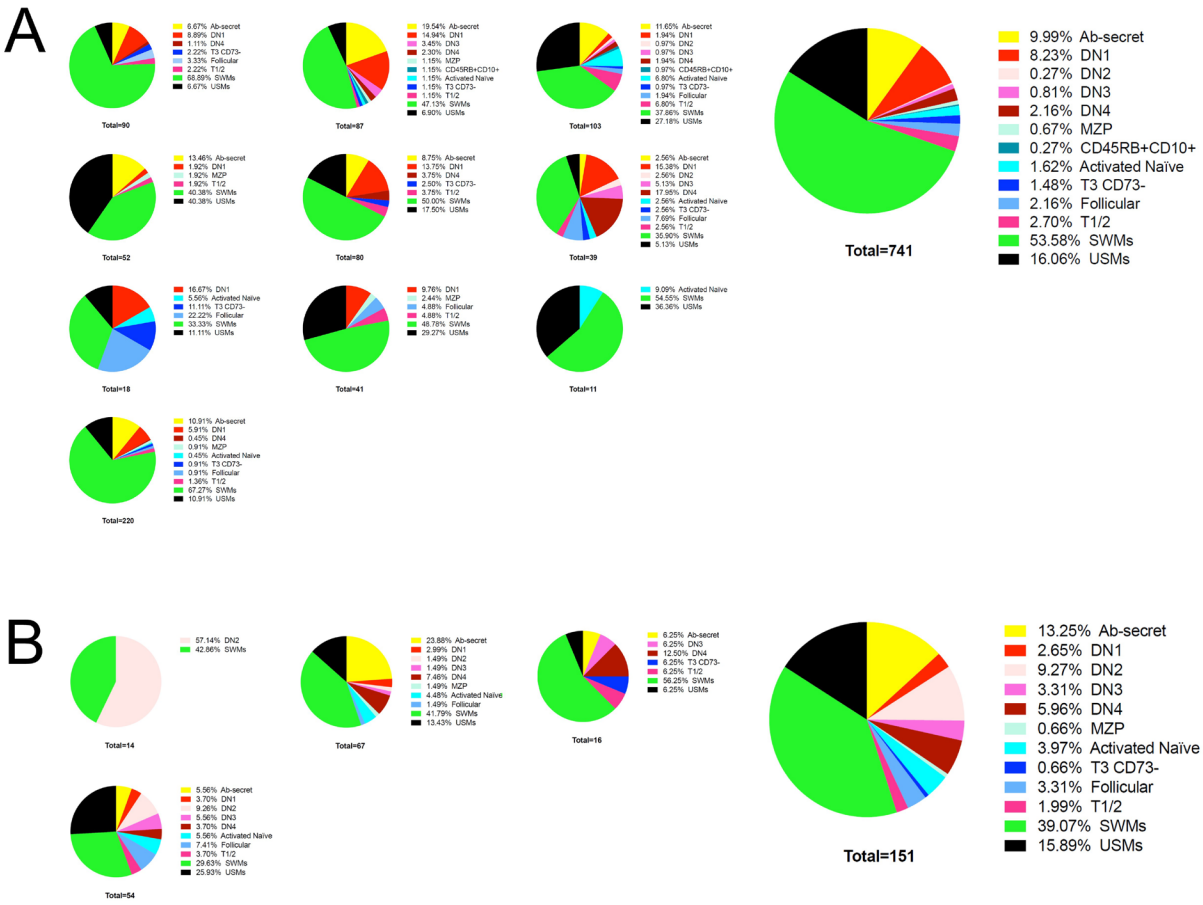

Fig. S7. CoV-2-RBD binding B cell subsets. All CD19+ B cells binding to CoV-2-RBD shown for (**A**) convalesced COVID-19 patients (n=10) and (**B**) hospitalized COVID-19 patients (n=4). Total reactive CD19+ B cells per patient (small plots) and summation of all CoV-2-RBD binding B cells per clinical criteria (large plots) shown. Antibody-secreting (Ab-secret), double negative (DN), marginal zone precursor (MZP), switched memory (SWM), transitional (T), unswitched memory (USM).